INFRARED FOCAL PLANE PERFORMANCE IN THE SOUTH ATLANTIC ANOMALY

FINAL REPORT

CONTRACT NO. NAS2-12898

SEPT. 30, 1989

To

NASA/AMES RESEARCH CENTER

From

LOCKHEED MISSILES & SPACE COMPANY, INC.
RESEARCH & DEVELOPMENT DIVISION
PALO ALTO, CA

CONTENTS

ILLUSTRATIONS

Figure

Page

TABLES

Section 1

SUMMARY

Proton-induced pulse height distributions (PHDs) in Si:XX detectors were studied analytically and experimentally. In addition, a preliminary design for a flight experiment to characterize the response of Si:XX detectors to the trapped proton environment and verify PHD models was developed.

PHDs were computed for two orbit altitudes (200 and 900 km) for a variety of shielding configurations (1 to 19.3 gm/cm^2). Most of the proton-induced pulses have amplitudes less than about 3.5 $\times$ 10^5 e-h pairs. Shielding has a small effect on the shape of the PHDs (for practical cases). The primary effect of shielding is to reduce the total number of pulses produced.

Proton-induced PHDs in a Si:Sb focal plane array bombarded by a unidirectional 67-MeV beam were measured. The maximum pulse height recorded was 6 $\times$ 10^5 pairs. The distribution had two peaks; the larger peak corresponded to 3.8 $\times$ 10^5 pairs and the smaller peak to 1.2 $\times$ 10^5 pairs. The maximum pulse height and the larger peak are within a factor of two of predicted values. The low-energy peak was not expected, but is believed to be an artifact of inefficient charge collection in the detector.

The planned flight experiment will be conducted on a shuttle flight. The Lockheed Missiles & Space Company, Inc., helium extended life dewar (HELD) will be used to provide the required cryogenic environment for the detector. Two bulk Si:Sb arrays and two Si:As impurity band conduction arrays will be tested. The tests will be conducted while the shuttle passes through the South Atlantic Anomaly. PHDs will be recorded and responsivity changes tracked. This experiment will provide a new database on proton-induced PHDs, compare two infrared-detector technologies in a space environment, and provide the data necessary to validate PHD modeling.

Section 2

INTRODUCTION

The major tasks in this program were theoretical and experimental investigations of the effects of trapped protons on the operation of infrared detectors in the South Atlantic Anomaly (SAA) and the design of a flight experiment to enlarge the database on proton effects on infrared focal plane arrays (FPAs) and validate proton pulse height models. The theoretical efforts were development of a PHD code and application of the NOVICE code to the computation of PHDs. In the experimental portion of the program, Si:Sb detectors were irradiated with 67-MeV protons, and radiation-induced signals were collected and analyzed. Before discussing the results of these studies, we present a brief phenomenological discussion of the problem. The flight experiment design will be discussed in a later section.

Ionizing particle radiation, such as that encountered in the trapped radiation belts and in strategic engagement, produces random pulses in the outputs of optical and infrared detectors. These pulses can be a significant source of noise. The number of noise electrons N generated in the detector in time τ is

$$N = \sqrt{\bar{n}\ \overline{\lambda^2}\tau}$$

where $\bar{n}$ is the average pulse generation rate and λ is the number of hole-electron pairs produced per interaction in the detector. n is assumed to be Poisson distributed and λ is a random variable. The probability of a pulse of a given magnitude being generated (the PHD) is a function of the particle type and energy, the detector geometry, and the type and quantity of material surrounding the detector. The pulse generation rate (event rate) depends on these quantities and on the particle flux density.

The pulse event rate due to charged particles, e.g., electrons, protons, and alphas, is a straightforward though difficult calculation. After accounting for the particles' energy losses in the detector surroundings, the PHD for an isotropic flux is obtained by a convolution of the

detector chord length distribution with the particle flux energy loss distribution. Some useful order-of-magnitude estimate, however, can be obtained from simple phenomenological arguments.

The proton-induced event rate, Er, in a single detector element is

$$E_r = \phi_p(\ell w + \ell t + wt)/2 \quad \text{events/s}$$

where ϕ_p is the isotropic proton flux density and l, w, and t are the detector dimensions. Each event produces a pulse of electron hole pairs N_p

$$N_p = (C/\epsilon)dE/dX \quad \text{(pairs)}$$

where C is a chord length, ϵ is the energy required to create an electron hole pair (3.65 eV in Si), and dE/dX is the energy loss rate of the proton. The average pulse height can be estimated by inserting average values for the quantities in the above equation. Typical dimensions of a bulk extrinsic Si detector pixel are $75 \times 75 \times 300\ \mu^3$. The peak proton flux density in a 300-km circular orbit (28° inclination) is about $200/cm^2$-s. This flux density will produce an event rate of 0.05 events/s per pixel. A significant fraction of the total proton flux falls in the 50- to 200-MeV range. The average proton energy loss rate in that energy interval is 1.2×10^3 eV/μm. The average chord length of the detector is about 75 μm. The average value of the PHD should be about 2.5×10^4 pairs. Noise levels at the detector array output of less than 200 electrons (rms) can be achieved. Thus, during a 500-s integration time, one expects about 25 events which exceed the detector noise level by about 1000 times. These events, due to their frequency and magnitude, significantly reduce the performance of the detector.

Section 3

RESULTS

In this section we present the results of both our analytical work on calculating pulse height distributions and the results of the cyclotron tests on an Si:Sb FPA.

3.1 PULSE HEIGHT DISTRIBUTION CALCULATIONS

The calculation began with the computation of the chord length distribution of a detector. The starting point was a paper by Bradford (J. Appl. Phys., Vol. 50, 1979, p. 3799), which gives a general expression for the sum distribution of chord lengths in a rectangular parallelepiped. The chord length distribution is the negative derivative of the sum distribution with respect to the chord length. Several mistakes were found in Bradford's paper and were corrected (see Appendix A). The final results for the sum distribution may be determined by analytical evaluation of integrals or by numerical integration of intermediate expressions. Both techniques were used to reproduce one of Bradford's results. The numerical integration technique gave the better results. The failure of the analytical technique is believed to be related to roundoff errors since the expressions are very long and complicated.

At this point in the program we acquired the NOVICE code, a mature Monte Carlo transport code which had been used elsewhere to compute pulse height distributions in detectors. Further development of our own pulse height distribution code was halted for reasons of economy.

The NOVICE computer program is basically a particle transport and shielding calculation code. Our particular use of the many features of the NOVICE program has been to calculate pulse height distributions (PHDs) for Si detectors within a spherical shield exposed to an isotropic proton flux. Proton flux densities appropriate to the SAA were used. The energy distribution of the proton flux was separately calculated using the AP8MIC model. NOVICE performs a Monte Carlo simulation of sensor irradiation with randomly selected incident proton energy and angle of approach to the detector.

Through a series of input data sections the user defines the Si sensor and shield configurations. The detector investigated was a centrally located detector in a 58 $\times$ 62 Si detector array. The array was 300-μm thick and each pixel was 75 $\times$ 75 μ^2. The detector array was In bump bonded to a Si readout chip (500-μm thick). The whole array was mounted on a Cu heat sink. The array and heat sink were surrounded by a spherical shell 1-cm thick; the effect of shield material was investigated. The user defines the desired output of the program: in this case, the range of the calculated pulse height spectrum. Pulse heights are given in energy deposited per event. To convert energy (in eV) to electron hole pairs, divide the pulse height by 3.65.

Pulse height data are accumulated and output to a special file at the end of the calculations. This file is available for display or further analysis. Output data are in units of the number of events (energy spikes) within each designated subrange of the pulse height spectrum, normalized to the incident radiation flux. To obtain the count density, we divide each count output of the NOVICE program by the width of its respective energy interval.

The uncertainty of the results due to taking a finite number of incident particle samples in the Monte Carlo simulation process are displayed in the PHD figures by plotting the mean value and the +/– one standard deviation value. Higher energy values are subject to greater uncertainty than lower energy values for a given scenario, because fewer of the randomly selected incident particles yield pulses in the higher energy range.

We first investigated the effect of proton energy and shielding density on PHDs from some simple spectra. The results of calculations are easily related to phenomenological models and provide a good check on the operation of NOVICE. Three quasi-monochromatic uniform isotropic proton energy spectra were used: 48 to 52 MeV, 68 to 72 MeV and 98 to 102 MeV. A 1-cm shield of density either 1 gm/cm^3 or 2.7 gm/cm^3 surrounded the focal plane array. The resultant PHDs are shown in Fig. 3-1. The lower energy input spectra produce larger pulses than the highest energy spectrum. The maximum energy a 98-MeV proton can deposit in the detector is about 0.5 to 1 MeV (taking into account the energy loss in the 1-cm-thick shield). Since the proton energy loss rate decreases with increasing energy, this shift in PHD is expected. The lower portion of the PHD is not as strongly dependent on proton energy; however, the steep portion of the distribution does move toward larger pulse amplitudes with decreasing proton energy.

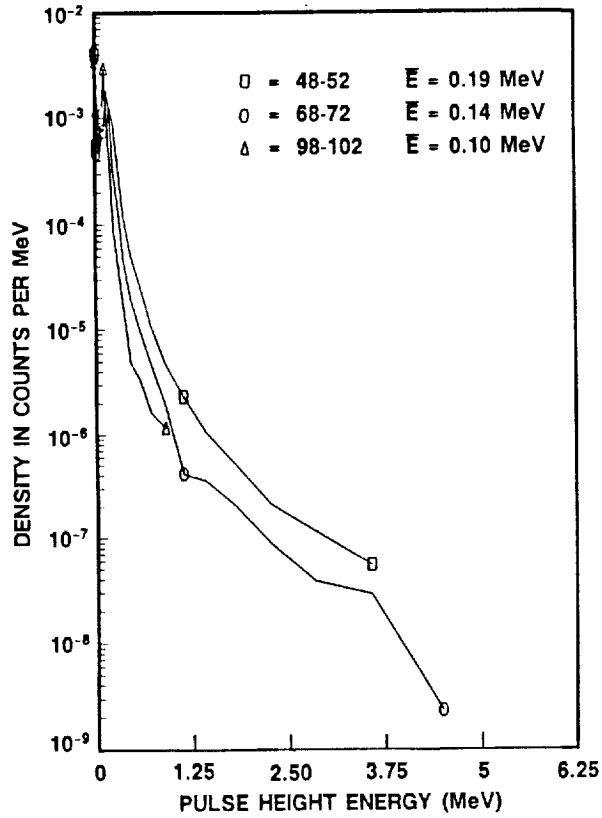

Fig. 3-1 Normalized PHD, Density 1 Shield, Narrow-Band Incident Spectra

Increasing the density of the shielding material should have the same effect as lowering the proton energy. This is observed (see Figs. 3-2, 3-3, and 3-4). The peak energies of the energy-degraded spectra are 39, 45, and 82 MeV. We note that the energy-degraded 68- to 72-MeV spectrum produces a PHD very similar to the undegraded 48- to 52-MeV spectrum (compare Figs. 3-1 and 3-3).

The mean chord length $\bar{c}$ of a rectangular parallelepiped is

$$\bar{c} = \frac{2\ell wh}{\ell w + \ell h + wh}$$

The mean chord length of a 75- × 75- × 300-μ^3 detector is 67 μ. The energies deposited by the mean energy proton in each of the three spectra are: 1.5×10^5, 1.2×10^5, and 8.9×10^4 eV for the 48- to 52-, 68- to 72-, and 98- to 102-MeV spectra, respectively. These mean energies and their trends with energy compare well with the result of the NOVICE calculations (Table 3-1). The higher pulse count for the $\rho = 2.7$ shield relative to the $\rho = 1$ shield is believed to be due to a softening of the proton energy spectrum by the denser shield.

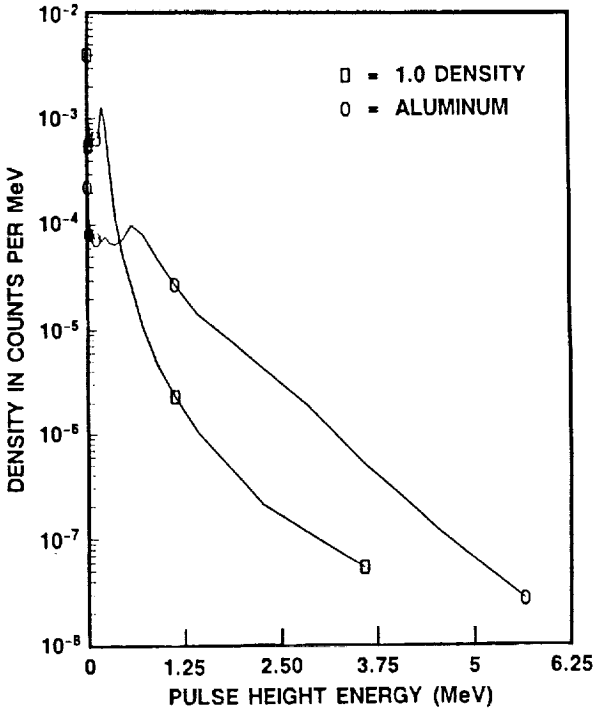

Fig. 3-2 Normalized PHDs for 48- to 52-MeV Input Spectrum

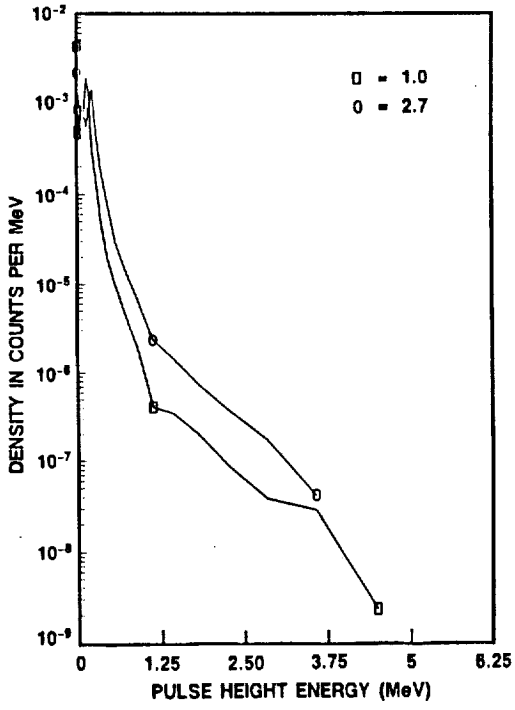

Fig. 3-3 Normalized PHDs for 68- to 72-MeV Incident Spectrum

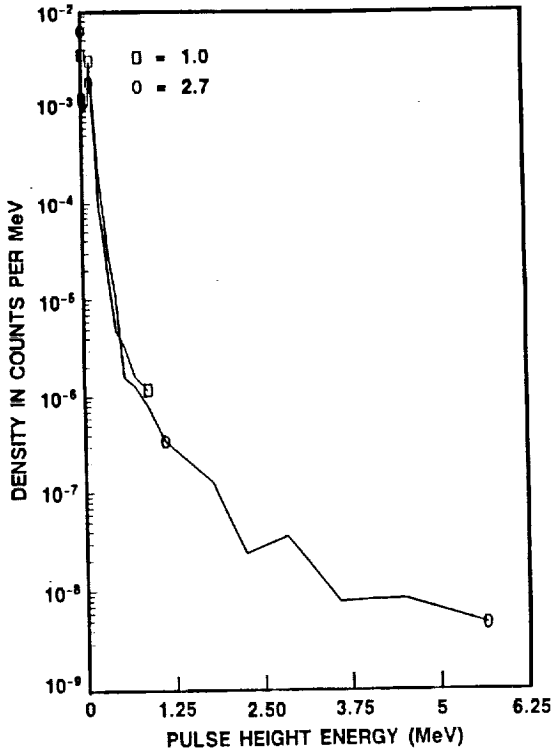

Fig. 3-4 Normalized PHD, 98- to 102-MeV Incident Spectrum, Shield Densities 1.0, 2.7

Table 3-1 SUMMARY OF PHD CHARACTERISTICS FOR QUASI-MONOCHROMATIC PROTON FLUXES

Energy Band (MeV)	Mean of PHD (MeV) Shield Density		Variance of PHD Shield Density		Relative Number of Pulses*
	$\rho = 1$	$\rho = 2.7$	$\rho = 1$	$\rho = 2.7$	
48-52	0.19	0.72	0.028	0.37	1.4
68-72	0.14	0.21	0.014	0.033	1.6
98-102	0.10	0.12	0.005	0.009	1.2

$$\text{*Relative Number of Pulses} = \frac{\text{Total Number of Pulses for } \rho = 2.7 \text{ Shield}}{\text{Total Number of Pulses for } \rho = 1 \text{ Shield}}$$

PHDs for two trapped proton spectra were calculated for different shield densities. The PHDs from these broader energy spectra are more complex and difficult to interpret. The proton spectra for 300-km and 900-km circular orbits with 28° inclinations were computed using AP8MIC. These two energy spectra are summarized in Table 3-2.

PHDs were computed for four shield configurations: 1-cm shield (ρ = 1, 2.7, 19.3) and an Al-Ta-Al combination (2.5×10^{-2} cm Al + 0.1 cm Ta + 0.23 cm Al).[1] This latter shield configuration was chosen because it effectively removes trapped electrons. The minimum shielding configuration (1 cm of 1 gm/cm^3 material) is well below minimum shielding configuration for any practical case. The 1 cm of 2.7 gm/cm^3 material corresponds to the expected shielding configuration in the planned flight experiment. The effects of slight perturbation in the proton energy spectra were also investigated by uniformly shifting the

Table 3-2 ORBITAL PROTON ENERGY DISTRIBUTIONS

Proton Energy (MeV)	Relative Number Protons/MeV in Each Band	
	300 km	900 km
4 - 6	1.13×10^{-2}	8.4×10^{-3}
6 - 10	1.15×10^{-2}	7.4×10^{-3}
10 - 15	8.2×10^{-3}	7.7×10^{-3}
15 - 30	6.23×10^{-3}	6.33×10^{-3}
30 - 50	5.65×10^{-3}	5.00×10^{-3}
50 - 70	5.57×10^{-3}	4.88×10^{-3}
70 - 90	4.50×10^{-3}	4.22×10^{-3}
90 - 110	4.47×10^{-3}	3.93×10^{-3}
110 - 150	3.68×10^{-3}	3.31×10^{-3}
150 - 200	2.15×10^{-3}	2.26×10^{-3}
200 - 250	1.32×10^{-3}	1.52×10^{-3}
250 - 300	6.96×10^{-4}	9.78×10^{-4}
300 - 350	3.76×10^{-4}	6.3×10^{-4}
350 - 400	2.06×10^{-4}	4.08×10^{-4}
400 - 450	1.86×10^{-4}	7.54×10^{-4}

input spectra by ± 0.25 MeV. Characteristics of the computed PHDs are summarized in Table 3-3.

The general trends of all the PHDs computed are well illustrated by Figs. 3-5, 3-6, 3-7, and 3-8 for the 900-km input spectrum and the four shielding configurations. The shielding effects at low-pulse amplitudes can more easily be seen in Fig. 3-9.

Increasing shield density primarily affects the number of pulses produced. According to Table 3-3, the total number of pulses (per unit incident flux density) decreases by a factor of 1.5 as the shield density increases from 1 to 19.3 gm/cm^3. This reduction occurs over the entire PHD.

The broad peak around 5 MeV is observed in all the PHDs computed using broadband energy input spectra. This peak is not the result of a distortion in the proton energy spectrum introduced by the shielding computation in NOVICE.

This was verified by computing the PHD for the case of no shielding and a truncated energy distribution. The high end of the energy distribution was truncated by energy corresponding to the energy absorption in the shield. This PHD displayed all the features of the PHD shown.

A series of diagnostic PHDs was calculated using different energy input spectra and no shielding. The spectra were uniform over the following energy bands: 2 to 10, 2 to 30, 2 to 60, and 2 to 200 MeV. The evolution of the PHDs with increasing proton energy can be seen in Fig. 3-10. Consider first the 2- to 10-MeV spectrum case. The highest energy pulse is produced by a proton whose range is just equal to the longest chord length of the detector (320 mm). Higher-energy protons have a lower-energy ion rate and therefore deposit less energy along this chord.

Lower-energy pulses will be produced by both higher-energy protons and lower-energy protons. For example, a 10-MeV proton (whose range is about 770 μm) will deposit 2.6 MeV along the longest chord. A 2-MeV proton will deposit all its energy in 25 μm. Thus, the low end of the PHD can be attributed to both low- and high-energy protons.

Figure 3-11 shows the chord length sum distribution and chord probability density for a 75- × 75- × 300-μ^3 detector. Note that 50% of the chords have lengths greater than 75 μm (the range of a 2.5-MeV proton). Thus, low-energy protons will be effectively absorbed, producing pulses in the MeV range.

Table 3-3 SUMMARY OF ORBITAL FLUX SPECTRA PHD CHARACTERISTICS

					Energy Distribution Shifted By (MeV)			
					+0.25	−0.25	+0.25	−0.25
300-km Orbit								
Shielding Density (gm/cm^3)	ρ = 1	ρ = 2.7	19.3	Al-Ta-Al	ρ = 1		ρ = 2.7	
Mean Energy (MeV)	0.11	0.10	0.109		0.096	0.13	0.09	0.12
Variance	0.035	0.027	0.032		0.026	0.05	0.023	0.036
Total Number of Pulses	2.6×10^{-5}	2.2×10^{-5}	1.7×10^{-5}		2.4×10^{-5}	3.1×10^{-5}	2×10^{-4}	2.4×10^{-5}
900-km Orbit								
Mean Energy	0.098	0.09	0.095	0.09	0.09	0.12	0.08	0.11
Variance	0.028	0.022	0.025	0.025	0.023	0.042	0.02	0.029
Total Number of Pulses	2.4×10^{-5}	2×10^{-5}	1.7×10^{-5}	2.1×10^{-5}	2.2×10^{-5}	2.2×10^{-5}	1.9×10^{-5}	2.9×10^{-5}
n/no	1	0.83	0.71	0.875	0.91	0.91	0.79	1.2
$\frac{\Delta^2 r}{no}$	0.038	0.025	0.024	0.029	0.028	0.05	0.021	0.049

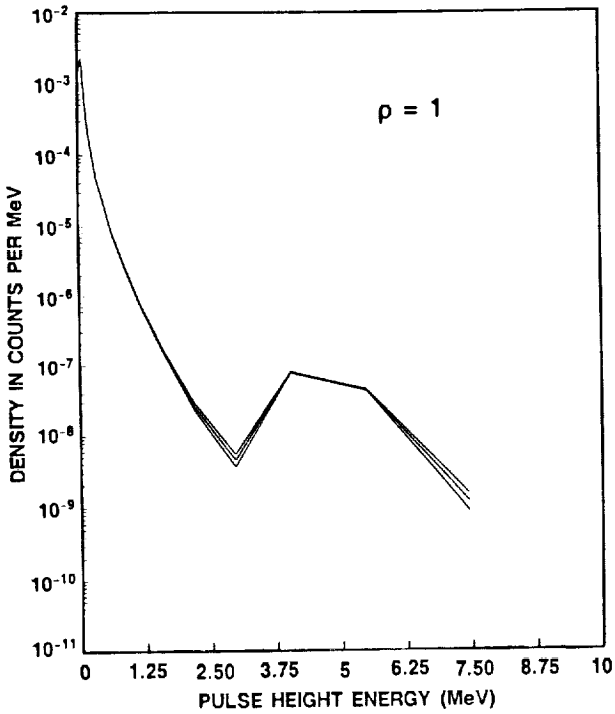

Fig. 3-5 Normalized PHD, 900-km Spectrum, ρ = 1

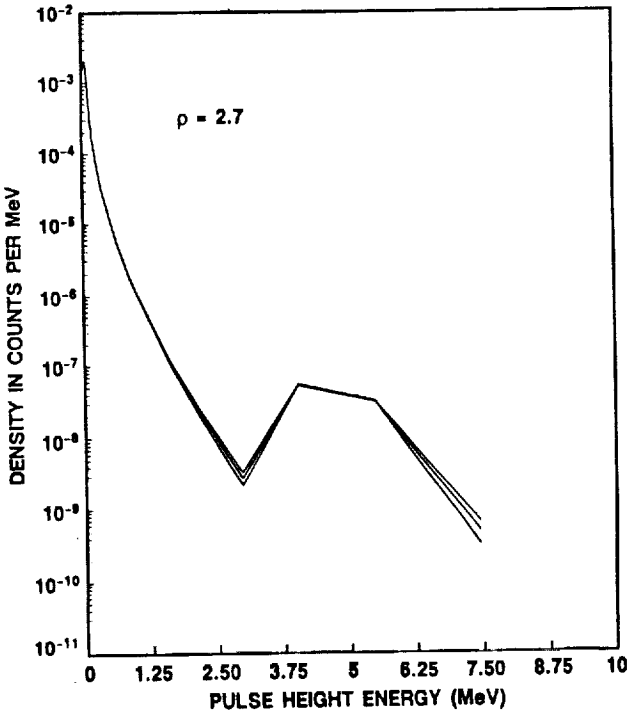

Fig. 3-6 Normalized PHD, 900-km Spectrum, ρ = 2.7

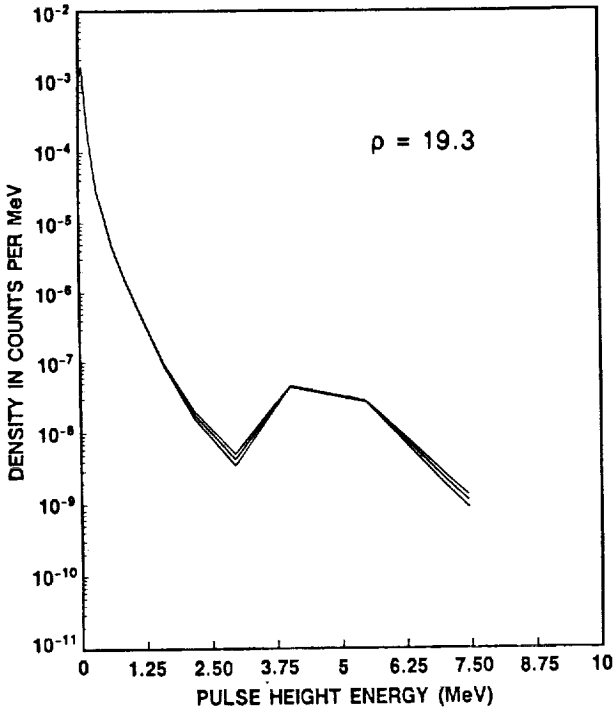

Fig. 3-7 Normalized PHD, 900-km Spectrum, 1-cm Tungsten Shield

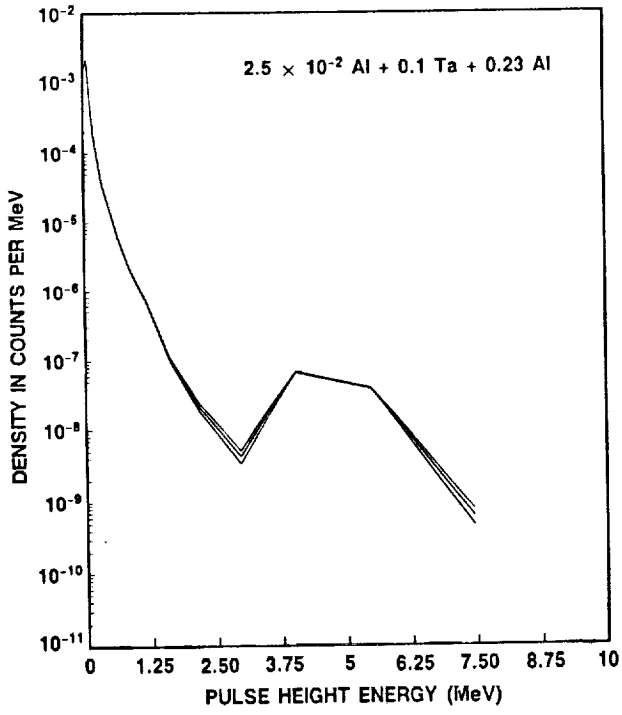

Fig. 3-8 Normalized PHD, 900-km Spectrum, Al-Ta-Al Shield

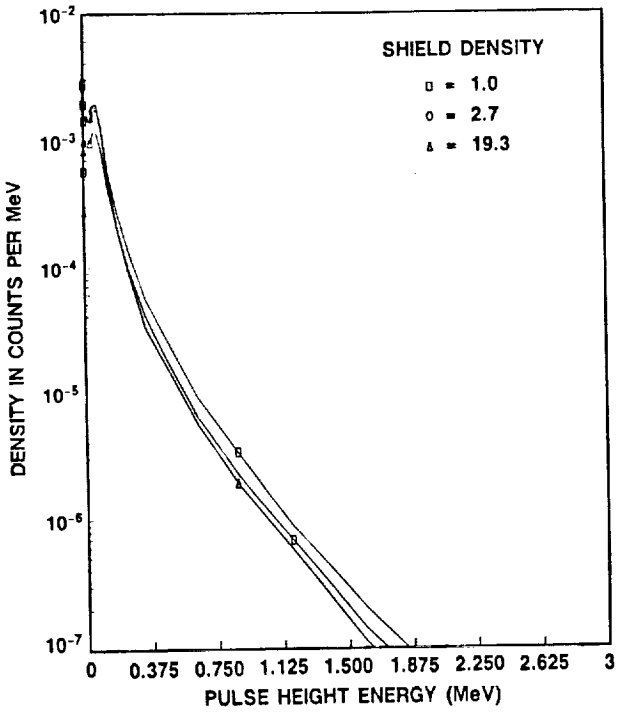

Fig. 3-9 Normalized PHD, 300-km Spectrum, 1-cm Shield

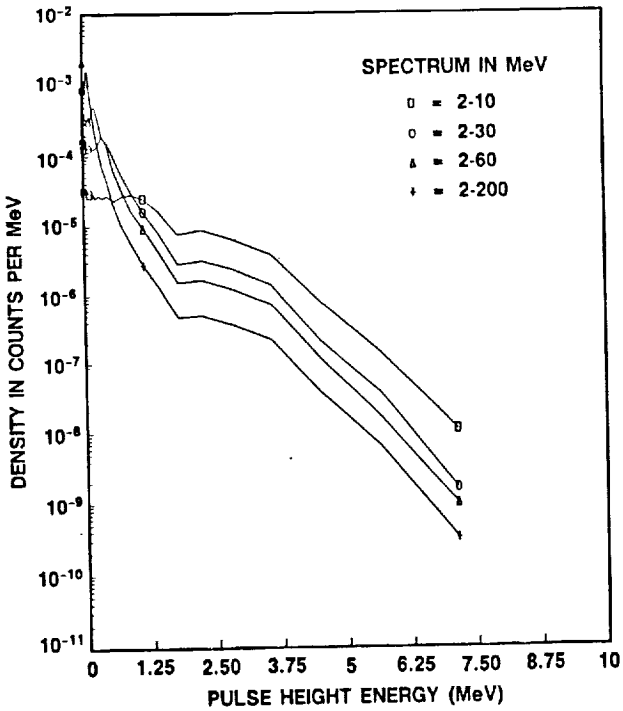

Fig. 3-10 Normalized PHD, No Shield, Various Flat Spectra

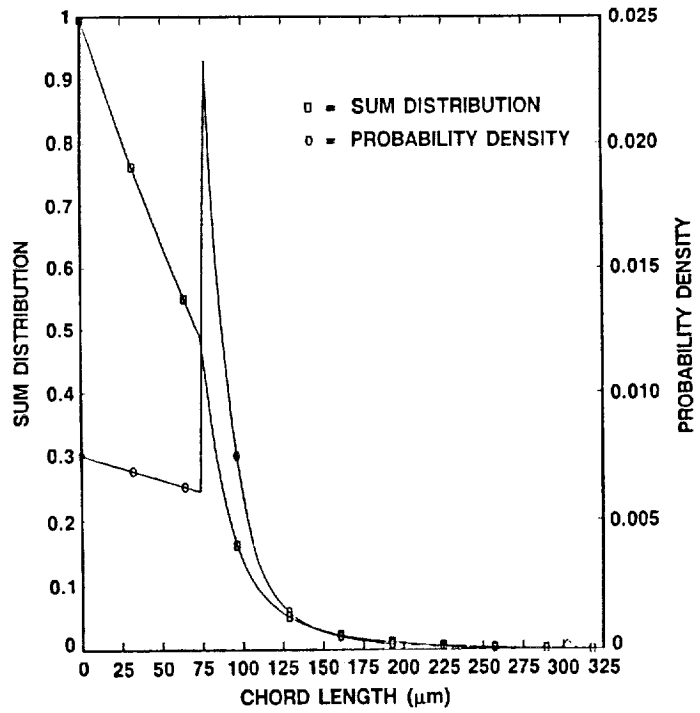

Fig. 3-11 Chord Length Distribution, 75- × 75- × 300-μm Volume

As higher-energy protons are added to the spectrum, the low-amplitude pulse density increases. These protons have ranges far in excess of any chord length and therefore produce small pulses. The PHD for the 2- to 200-MeV spectrum is very similar to the PHDs in Figs. 3-5 through 3-8, including a shallow trough at about 1.25 MeV. The depth of the trough in Fig. 3-8 may be due to the detailed shape of the proton distribution after passing through the shielding material. Recall that there was no shielding in the cases shown in Fig. 3-10.

In summary, it is clear from these calculations that shielding reduces the total number of pulses produced in the detector. Large amounts of shielding (e.g., 19.3 gm/cm^2) do not significantly reduce the number of pulses. This is due to the fact that most of the pulses are the result of interactions with high-energy protons which cannot be shielded against.

Shielding and fluctuations in the trapped proton energy distribution can affect detector noise. Mandel (Brit. J. Appl. Phys., Vol. 10, 1959, p. 222) developed a formalism for calculating the noise associated with image fluctuations. The formalism is applicable to proton-induced noise processes in detectors. Consider n incident particles, each of which creates λ secondaries (λ is a random variable). We associate n with the incident proton and λ with the

number of electron hole pairs in a proton-generated pulse in the detector. The variance $\overline{\Delta^2\mu}$ in the number of electron-hole pairs produced is

$$\overline{\Delta^2\mu} = \bar{\lambda}^2\overline{\Delta^2 n} + \bar{n}\overline{\Delta^2\lambda}$$

where the variances all have the form

$$\overline{\Delta^2\mu} = \overline{\mu^2} - \bar{\mu}^2 \text{ etc.}$$

This holds for any distribution of n and λ. Adding shielding changes all the quantities on the RHS. In addition, a perturbation in the trapped photon energy spectrum will affect all the parameters in the equation. A fluctuating energy spectrum will add a new noise term. We can use the data in Table 3-3 to investigate the effect of shielding and energy distribution fluctuation on noise.

In making these comparisons, it is convenient to equate the total number of pulses to $\bar{n}$ and to divide $\overline{\Delta^2\mu}$ by $\bar{n}_o$, the total number of pulses for the $\rho = 1$ shielding case. In this way a direct comparison of each can be made. Since n is Poisson distributed, $\overline{(\Delta n)^2} = \bar{n}$, the above equation becomes

$$\frac{\overline{\Delta^2\mu}}{\bar{n}_o} = \frac{\bar{n}}{\bar{n}_o}\left[\bar{\lambda}^2 + \overline{\Delta^2\lambda}\right]$$

The results for the 900-km orbit are summarized in Table 3-4.

For a constant input energy distribution, shielding always reduces the noise. A small shift in the energy spectrum toward lower energies can increase the noise by as much as a factor of two. The noise is then very sensitive to the actual proton distribution, and fluctuations in the spectrum will produce a new noise term.

3.2 FPA IRRADIATION TESTS

Proton irradiations of a Si:Sb FPA were made at the University of California at Davis (UCD) cyclotron facility. A photograph of the 58 × 62 array is shown in Fig. 3-12. The detector array is In-bump bonded to a switched field-effect transistor (FET) multiplexer readout circuit. A schematic diagram of the circuit is shown in Fig. 3-13. The FPA was contained in the Ames

Table 3-4 IMPACT OF SHIELDING AND ENERGY SPECTRUM ON NOISE

Shielding					Shifted Energy Distributions			
					ρ = 1		ρ = 2.7	
ρ =	1	2.7	19.3	Al Ta Al	+0.25	−0.25	+0.25	−0.25
n/no	1	0.83	0.71	0.88	0.91	0.91	0.79	1.2
$\frac{\overline{\Delta^2\mu}}{no}$	0.038	0.025	0.024	0.029	0.028	0.05	0.021	0.049

"Cryotran" test dewar (Fig. 3-14). A block diagram of the test electronics is shown in Fig. 3-15. Pre-experiment testing and evaluation of the FPA were performed by the NASA Ames personnel. Both the dark can and the vacuum jacket had thin Al windows. A 1-in.-thick Al plate with a 0.75-in. hole was placed immediately in front of the dewar vacuum window to define the proton beam. The proton beam traveled about 10 in. in air before entering the dewar. Two plastic scintillation counters were positioned in the air space. By using coincidence counting, an accurate determination of the proton flux density could be made. The proton beam energy was 67 MeV, a value chosen for reasons of beam control and stability.

One limitation of ground-based experimentation is that only monoenergetic or nearly monoenergetic particle beams are available. The pulse height distribution from such a beam is not, in itself, interesting. As an example of such an "uninteresting" distribution, we show the PHD generated by a uniformly distributed 40- to 60-MeV proton beam (Fig. 3-16). The PHD should consist of a single well-defined peak corresponding to the energy deposited along the length (interelectrode spacing) of the detector (for our normal incidence irradiations). Since the pulse peak is well defined, deviations from this ideal are readily observed. These deviations may be due to proton interactions in the FPA surrounding which produce secondary sources of ionizing radiation or charge collection anomalies in the detector array. Examples of secondary ionizing radiation fluxes are: K and L-shell x rays, bremsstrahlung,

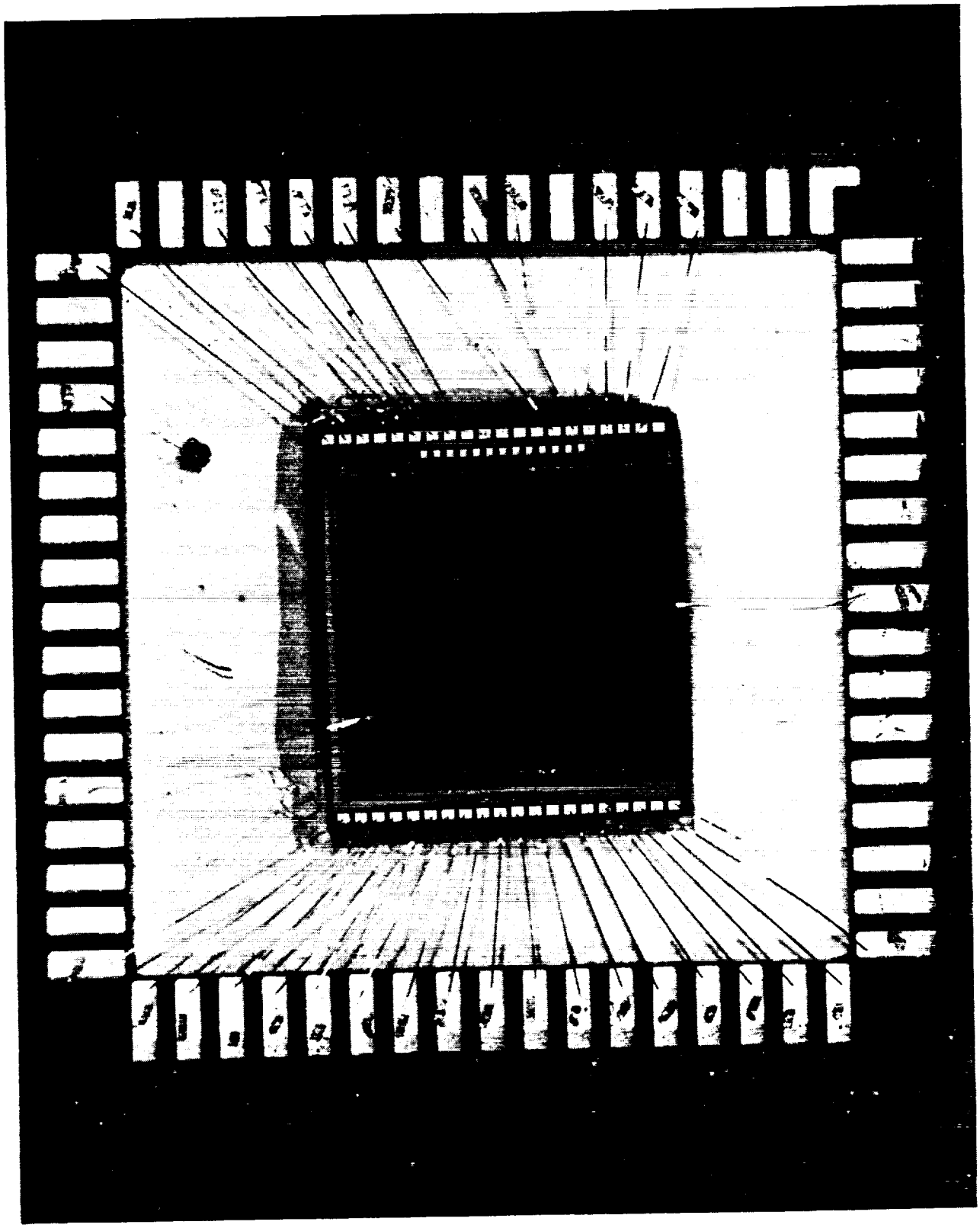

Fig. 3-12 58 x 62 Si:Sb Infrared Focal Plane Array

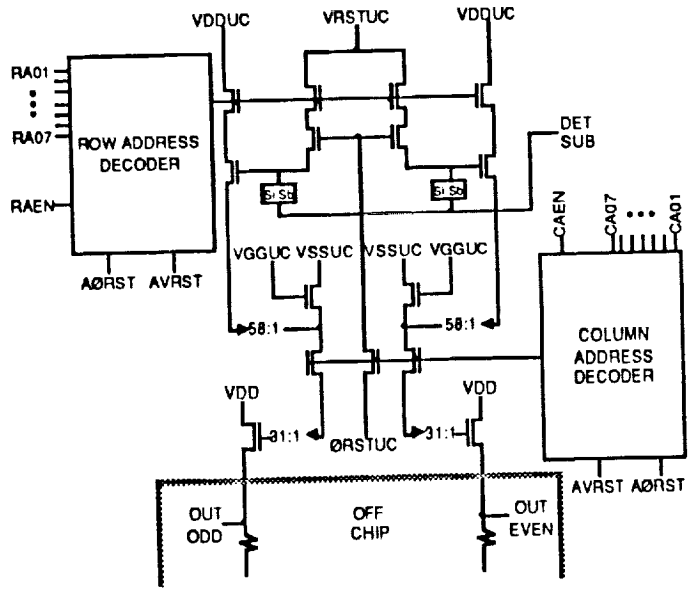

Fig. 3-13 Schematic Diagram of Multiplexer Unit Cell

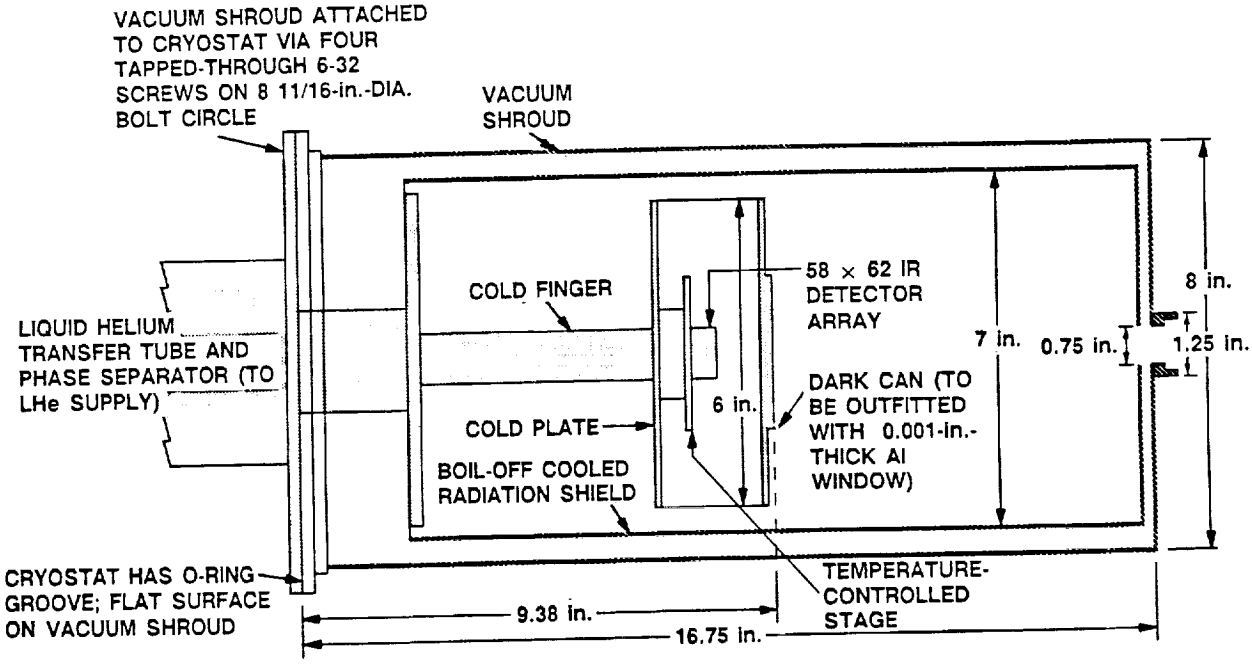

Fig. 3-14 Schematic View of Ames' "Cryotran" Test Dewar

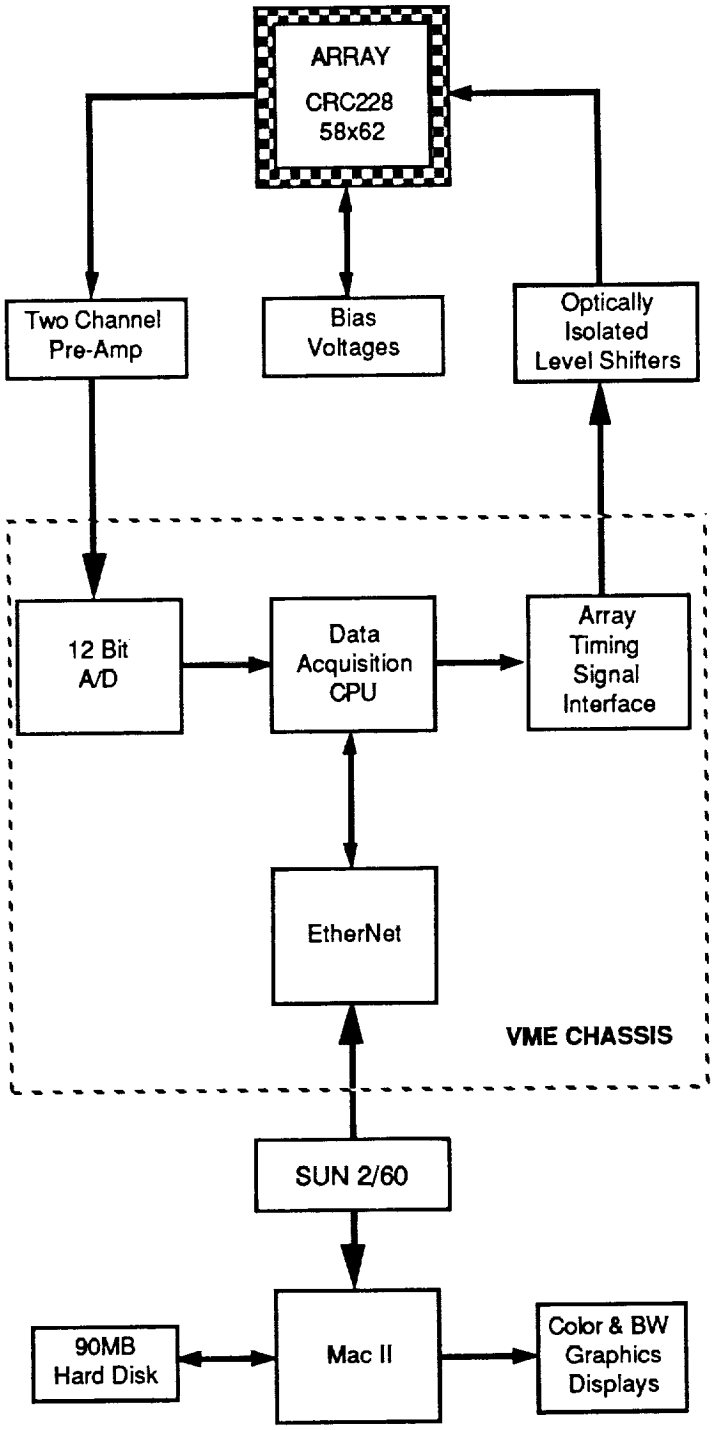

Fig. 3-15 Block Diagram of Test Electronics

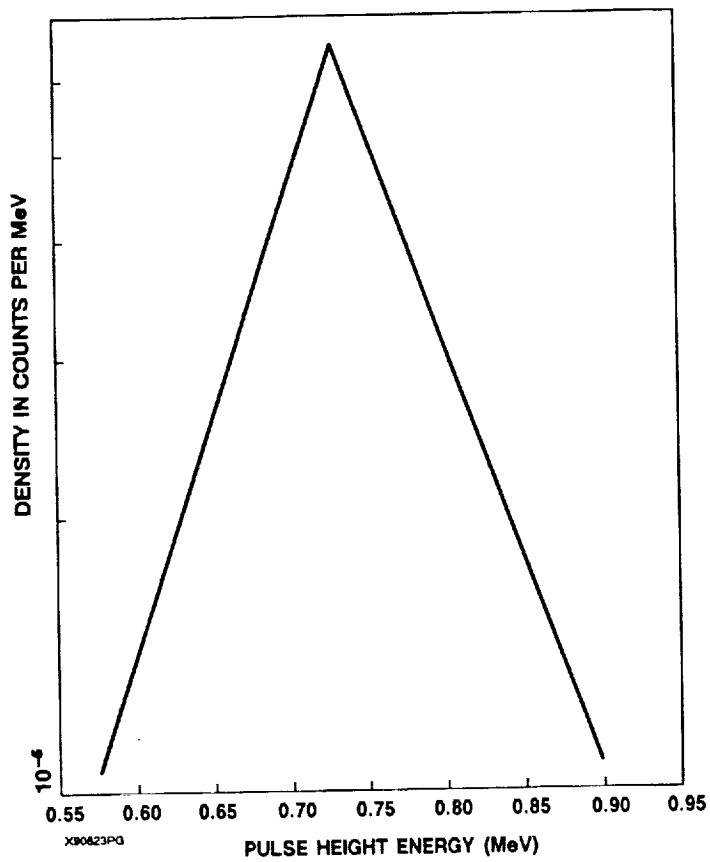

Fig. 3-16 Pulse Height Relative Distribution (Unidirectional)

and γ photons produced in the detector surroundings. Charge-collection anomalies include incomplete charge collection and charge sharing (i.e., blooming).

The objectives of these experiments were:

(1) Determination of the PHD for a well-defined (energy and angle of incidence) proton beam

(2) Observation of blooming due to the high density of deposited charge in a pixel

Coincidence pulses due to a proton traveling through two detectors would not be observed in our experiments.

The FPA used was fabricated by the Santa Barbara Research Center. The detectors were 300-μ thick with 75- $\times$ 75-μ^2 pixel areas. The Cryotran dewar, FPA, and electronics were supplied by NASA Ames.

The first cyclotron run produced no useful PHD data. The first proton hit caused the array to hang up at the supply voltage. With the beam off, the array could be reset. The first proton hit

after reset would initiate hang-up again. Post-irradiation diagnostics revealed that a combination of a low voltage on V_{gg} and a faulty FPA ground provided the necessary conditions for a proton-induced pulse to initiate hang-up.

In the second test, the output of a pixel well away from the edges of the array was monitored. A centrally located pixel was chosen to eliminate complications due to nonuniform collection fields which may be present at the edges of the array. In addition, it requires much less time to read out a single pixel than it does to read out the whole array. The objective was to collect as many data in as short a time as possible. From other studies we have found that in order to obtain statistically valid PHD, about 10^4 pulses need to be counted. Typically, 100 pulse height channels would be used. If 10^4 counts were uniformly distributed over all the channels, then a rms error of 10% in each channel is expected. In the case of a nonuniformly distributed PHD, the peak of the distribution will be defined with greater precision than the wings of the distribution.

Proton flux densities of 1700 and 4000 p/cm^2-s were used. Detection integration times were 16 or 32 ms. Table 3-5 is a matrix of the test conditions.

The number of events expected E_p is

$$E_p = \phi_p \; A_D \; \tau_i \; N_i$$

where

ϕ_p = proton flux density

A_D = detector area

Table 3-5 TEST CONDITIONS

Proton Flux Density	Integration Time		Samples Recorded at	
	16 ms	32 ms	16 ms	32 ms
1700	—	✓	0	2.8×10^4
4000	✓	✓	2×10^4	4.9×10^4

τ_I = integration time

N_I = number of integration samples collected

Table 3-6 summarizes the expected number of events expected for each combination of flux density and integration time.

The total number of events expected was about 510; the observed number of events was ~ 5300, over 10 times the expected value. The resulting pulse height distribution is shown in Fig. 3-17. The distribution is quasi-exponential with a peak pulse height of about 0.27 V. In this run, the amplifier gain, G, was 16 and the sense capacitance, C, was 7×10^{-14} f. The conversion of pulse voltage to pairs is

$$N_p = \frac{CV}{eG} \text{ pairs}$$

where e is the magnitude of the electronic charge.

The peak pulse contained 7.4×10^3 pairs and corresponds to an energy deposited of 2.7×10^4 eV (3.65 N_p). The largest pulse at 1.75 V contained 4.6×10^4 pairs (1.7×10^5 eV deposited). The energy loss rate for a 67-MeV proton in Si ($\rho = 2.33$ g/cm^3) is 1.9×10^7 eV/cm ("Studies in Penetration of Charged Particles in Matter," Barkas and Berger, National Acad. Sci., Nuclear Science Series, Report No. 39, 1964). The expected energy deposited in a 300-μm-thick detector is about 5.6×10^5 eV. The entire PHD is well below this expected value. The observed PHD is anomalous with respect to both number of events and the magnitude of the events. The excess number of pulses could be due to

Table 3-6 EXPECTED NUMBER OF PROTON EVENTS

ϕ_p	τ_I	
	16 ms	32 ms
1700	86	72
4000		350

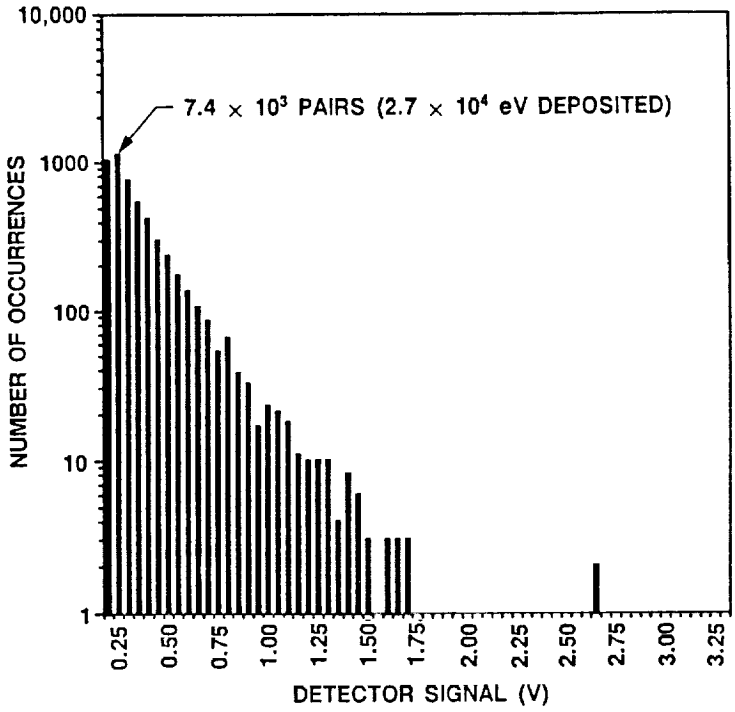

Fig. 3-17 Proton PHD (E_p = 67 MeV)

(1) Inaccurate dosimetry

(2) Extraneous sources of ionizing radiation produced by protons in the detector surroundings

(3) Collection of charge from adjacent pixels

(4) Events in the multiplexer

Because of the type of dosimetry used, we assume at this time that (1) is not a viable explanation.

Proton interactions in the array surroundings can result in the emission of ionizing radiation which may produce pulses in the detectors in addition to the pulses due to direct proton hits. These interactions can produce

- Bremsstrahlung
- X rays from K- and L-shell ionization events
- Gamma photons from nuclear interactions

The bremsstrahlung production rate is inversely proportional to the mass of the incident particle. Because of this dependence, the bremsstrahlung production rate by protons is always negligible compared to the production rate by electrons (R. B. Evans, The Atomic Nucleus, McGraw-Hill Inc., 1955, p. 600). The impact of trapped electron bremsstrahlung on the Shuttle Infrared Telescope Facility (SIRTF) focal plane array was investigated by Autio (NASA Report, Dec. 1975). He concluded that electron bremsstrahlung-induced pulse event rates were negligible compared to proton event rates in the detector. We concluded that proton bremsstrahlung-included events would not be observed.

Protons can ionize K- and L-shell electrons, resulting in the emission of x rays from the detector surroundings. A single proton can produce a shower of x rays which would affect a number of detectors in the array. Cross-section data for x-ray production by high-energy protons are not available. However, since the cross sections peak in the 1- to 2-MeV range and decrease at higher energies (E. Merzbacher and H. W. Lewis, Encyclopedia of Physics, Springer-Verlag, Berlin, 1958, p. 167), use of lower energy data will result in a worst case estimate of the effect. The maximum cross section for x-ray production in Al is 3×10^{-20} cm^2. Since the absorption coefficient of K- and L-shell x rays is on the order of 10^{-2} cm, only those protons interacting in the detectors' immediate surroundings will generate x rays which can reach the detector. The number of x-ray photons, I, per proton is

$$I = N\sigma\delta \quad \text{photons/proton}$$

where N is the atomic density of the material surrounding the detectors (Al), σ is the cross section for x-ray production in Al, and δ is the x-ray absorption length in Al. We find that I = 30. In our tests, the detector array was about 2 cm behind an Al cap. The maximum x-ray fluence at the array is about 1.2 x-ray photons/cm^2-proton. The Al K(alpha) emission occurs at 1.55 keV. Each x-ray photon will generate about 400 electron hole pairs. This effect could result in an increased number of small (relative to a direct proton hit) pulses in a detector output.

Cross sections for (p, gamma) reactions were calculated at UCD. The gamma photons produced in these interactions have energies in the 1- to 5- MeV range. These photons have meanfree paths of about 4 cm. Thus, gamma photons produced in the collimator can reach the detector array. The collimator will be the largest source of gamma photons since it totally absorbs a portion of the beam. To estimate the worst-case gamma flux density at the

detector, we assume that the proton beam is totally absorbed in the collimator and that no photons are absorbed by the dewar walls. The (p, gamma) cross section in Al at 67 MeV is 4.4×10^{-27} cm^2. The gamma flux density (G) at the array is

$$G = N\sigma\, t\phi_P A/(2\pi R^2) \quad \text{gamma photons/cm}^2\text{/s}$$

where N is the atomic density of Al, σ is the cross section, t is the thickness of the collimator (2.5 cm), ϕ_P is the proton flux density, A is the beam area (8 cm^2), and R is the collimator array separation (18 cm). Using these values, we find that $G = 2.6 \times 10^{-6}$. Clearly, this effect is negligible.

Option (3) is very attractive. The centrally located pixel is surrounded by eight pixels. We expect about 510 events in each pixel; therefore, in all nine pixels we would expect a total of about 4600 counts, close to the observed number. Pulses from adjacent pixels would be smaller than those originating in the central pixel, due to recombination. If we take the analogy of optical cross-talk, then these pulses should be about only 1% as large as the pulses from the central pixel. Thus, we would expect a PHD that is skewed toward small pulse heights.

The peak in the observed PHD corresponds to the energy deposited by a 67-MeV proton in 14 μm of Si. This distance is not unlike the distance of the sum of a p-n junction depletion width and a minority carrier diffusion length in a Si readout circuit. Thus, proton events in the readout circuit could be cited as the source of pulses observed (begging the question of what became of pulses due to events in the detector). However, since the nodal areas in the readout circuit are an order of magnitude smaller than detector areas, we would expect that this contribution to the PHD would be smaller than the contribution due to events in the detectors. This effect is then inconsistent with the observed event rate. It should also be noted that in Co^{60} irradiations of FPAs, few or none of the observed pulses can be attributed to interactions in the readout circuit.

In the third cyclotron irradiation test, the PHD was constructed from events in all pixels. Approximately 100 frames were recorded. These frames contained about 10^4 proton events. In these runs, detector bias was -5 V. The free field pixel signals were less than 200 mV. The data (thresholded at 2 V) are presented in Figs. 3-18 and 3-19. The data in the first figure were taken from the first 50 frames; the data in the second figure from the last 50

frames. Both PHDs terminate at about 11 V and have peaks at about 7 V. The gain in all cases is 8 and the sense capacitance is 7×10^{-14} F. The 7 V peak corresponds to the generation of 3.8×10^5 pairs (1.4-MeV deposited). The maximum value pulse contains about 6×10^5 pairs (2.2-MeV deposited). The PHDs have a low voltage peak at 2.25 V (1.2×10^5 pairs). Attempts to generate a PHD from a unidirectional monochromatic proton beam have not been successful. Only two points were computed after in excess 16 K Monte Carlo histories. The "triangular" PHD (Fig. 3-16) comes closest to representing the conditions existing when the data of Figs. 3-18 and 3-19 were taken. The peak in Fig. 3-16 is at an energy of 0.73 MeV (2×10^5 pairs); the pulse height at a frequency 100 times lower than the peak frequency is 1.4 MeV (3.8×10^5 pairs). These values are about a factor of two lower than those observed. However, since the computation did not exactly simulate the experimental conditions, the argument is considered satisfactory.

The simulation predicts a very symmetric PHD, in contrast to the observed spectra, which exhibit an additional peak at low energies. Other investigations using monochromatic gamma-ray sources have observed PHDs which are skewed toward low pulse heights (private communication, Mark McKelvey, NASA Ames). Figure 3-20 shows the response of a

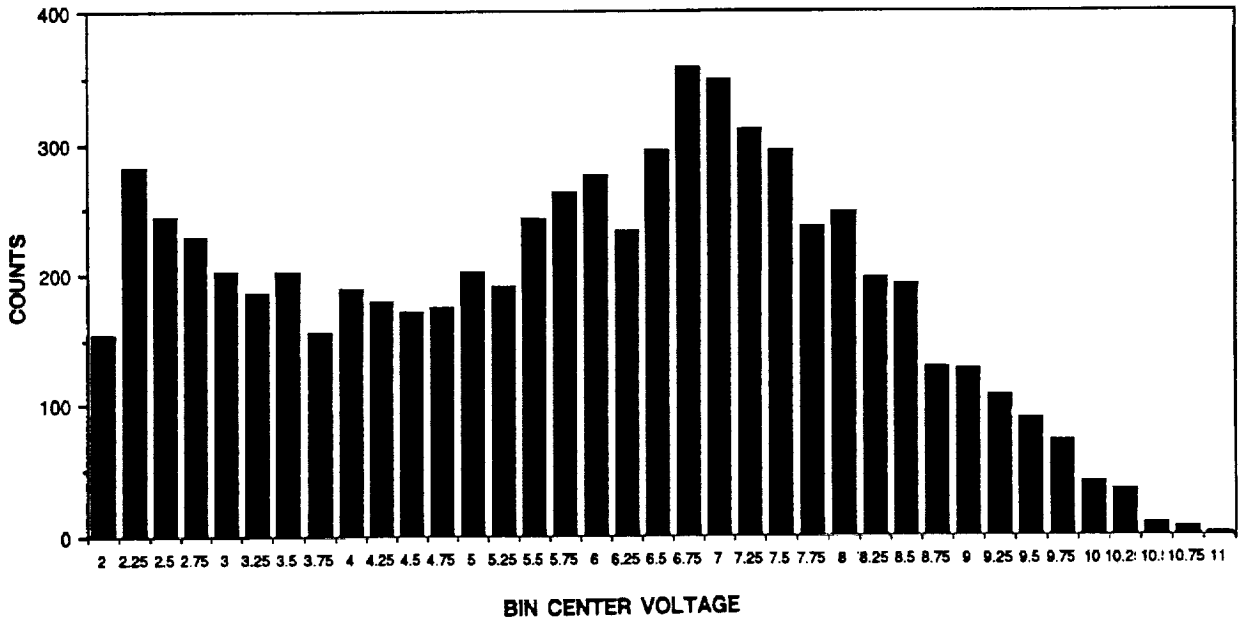

Fig. 3-18 PHD From Unidirectional 67-MeV Proton Beam (Sum of Frames 13-69)

Fig. 3-19 PHD From Unidirectional 67-MeV Proton Beam (Sum of Frames 70-112)

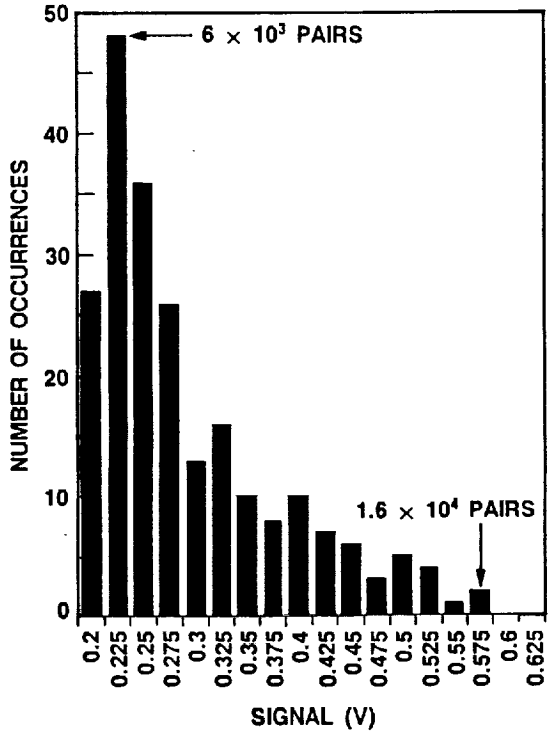

Fig. 3-20 Si:Sb Response to ^{241}Am Gamma Rays

Si:Sb detector array to 60 keV, ^{241}Am photons. The maximum voltage pulse at 0.575 V is due to a 1.6×10^4 pair pulse. This corresponds to 60 keV, the maximum energy the gamma ray can deposit. The preponderance of low-amplitude pulses suggest that the charge collection efficiency is incomplete and that most pixels have low charge-collection efficiencies. The same phenomenon may be active in the proton experiments producing the low energy peak.

Initial analysis of the data indicates that blooming does occur. However, blooming does not appear to extend beyond nearest neighbor pixels. In summary, the observed proton PHDs are in general agreement with computer predictions. The low energy peak is likely due to charge-collection inefficiencies in the detector rather than to an anomalous proton interaction.

Section 4
FLIGHT EXPERIMENT CONCEPT

In this section we describe a flight experiment whose objectives are to establish a database on proton-induced PHDs in Si:XX detectors, compare the response of bulk and impurity band conduction (IBC) detectors to proton bombardment, and validate proton-induced PHD modeling in Si:XX focal plane arrays. This flight experiment study was prepared within a framework based on the needs, goals, and limitations of the Outreach Program.

4.1 JUSTIFICATION FOR FLIGHT EXPERIMENT

SIRTF and some DoD missions plan to use Si:XX and other IR detectors. Depending on the orbit chosen, these detectors may pass through the trapped radiation belts. The trapped electron flux can be excluded with modest shielding; the proton flux cannot be shielded against. These protons will generate charge pulses on the order of 10^5 pairs in the detectors and will significantly degrade the signal-to-noise ratio of the detection system. In order to develop algorithms to reduce the effects of these pulses, their pulse height distribution must be known. Codes have been developed to compute the PHDs. However, the results of the codes have never been tested. Ground testing cannot accurately simulate the omnidirectional, energy-distributed proton flux encountered in space. A flight experiment provides the opportunity to test these codes. The validated PHD model then can be used with confidence to predict PHD in other detectors, e.g., InSb and HgCdTe.

Bulk Si:XX detectors have been in use for a number of years. IBC detectors are now available in limited numbers and are expected to replace bulk Si:XX detectors. This flight experiment would also provide an opportunity to compare the response of detectors of the two technologies in identical radiation environments. This experiment will enlarge our database on proton radiation effects in Si:XX detectors, provide needed PHD data, validate PHD modeling, and make a direct comparison of the responses of bulk and IBC detectors.

4.2 SUMMARY

The experiment will be performed on a shuttle flight. A 5-day experiment is planned. The experiment will require minimal attention by the flight crew (power on and power off only).

The experiment will be contained in the Lockheed Missiles & Space Company, Inc. (LMSC) project Helium Extended Life Dewar (HELD). The dewar will be mounted on one of the new extension capabilities of the Space Transport System (STS), the HITCHHIKER-M (HH-M). Some of the electronics will be mounted on the dewar. The remaining electronics will be stored in a sealed HH-G canister. Data will be collected during and after passage through the SAA and then down-linked using the medium-rate KU-band downlink. Data analysis will be performed on the ground by LMSC personnel. Another LMSC experiment (the Microsphere Investigation) will share the instrument space of the HELD. Since the focal plane experiment requires only 3.5 x 3.5 in., there is the possibility that a third experiment could be housed in the HELD instrument chamber.

Before describing the flight experiment hardware, we present a brief outline of the experiment protocol. The objectives of this experiment are to establish a database on trapped proton PHDs in two types of extrinsic Si detectors, validate pulse height prediction modeling, and assess long-term degradation effects. To obtain the largest possible database, the PHDs will be derived from the outputs of all the detectors on the FPA.

After achieving a stable orbit, the experiment electronics will be powered up. The experiment will contain its own computer to control measurement sequence. First, clear environment responsivity and noise measurements will be made (clear environment meaning outside the SAA. The FPAs will be operated continuously during passage through the SAA and all frames will be stored. After the third pass through the SAA, another clear environment check of responsivity and noise will be made. This agenda will be followed for the remainder of the experiment. Data will be downlinked as necessary. Periodically, after the post-SAA responsivity checks, the FPAs will be cycled to 15 K or higher to anneal out any total dose effects.

4.3 FLIGHT EXPERIMENT REQUIREMENTS

4.3.1 Data Requirements

The prime objective of this experiment is to gather statistically meaningful data on trapped proton-induced PHDs in infrared detectors of interest to NASA programs. The primary need is data fidelity. We must record a large number of pulses in order to achieve a statistically meaningful sample. Data and focal plane requirements appropriate to Si:XX detectors will be used in the following discussion. Similar requirements will apply if other detector technologies, e.g., InSb or Ge:Ga, are incorporated in the experiment.

A 300 km orbit was chosen for this discussion. The results will not be significantly different if the experiment were performed in a 900 km orbit. The AP8MIC model was used to calculate proton flux density and energy distribution. The total number of protons of all energies encountered in the SAA in 1 day is 2.38×10^5 P/cm^2. Typical effective areas of bulk Si:XX detectors are about 2.5×10^{-4} cm^2 (75-μm × 75-μm × 300-μm detector). A single pixel would experience about 60 proton hits/day. An IBC detector with the same optical area would receive about four times fewer proton hits. Since our experiment will last only a few days, this approach cannot provide the 10^4 data samples we require. If, however, we read all the FPA pixels, then we will obtain about 2×10^5 data points/day in a bulk technology FPA and about 4×10^4 data points/day in an IBC technology array (each array will contain 58 × 62 elements). Thus, in order to achieve the needed database, the PHD will be constructed from the data from all the pixels on the FPA. This is not an optimum experimental design since edge pixels may have a different response to protons than do interior pixels (due to different fringing electric fields around the pixels). However, these external pixels constitute less than 10% of the total pixel population. We believe that this tradeoff between number of data points and absolute fidelity is required for a viable experiment.

Total dose effects due to protron bombardment are not of major interest in this experiment. These experiments can be adequately performed on the ground. The total dose in the course of this mission will be small. A single 50-MeV proton deposits about 3×10^{-3} r/pixel hit. Therefore, a single pixel will accumulate about 0.5 r per day. If the flight lasts 5 days, the total dose will be about 2.5 r. Total dose effects at 1 r have been observed in ground tests. Thus, these measuremets may be significant.

4.3.2 FPA Characteristics and Requirements

Extrinsic silicon infrared detectors are strong candidates for IR astronomy applications such as SIRTF. Such detectors can be doped with In, Bi, As, Ga, or Sb to achieve various spectral band coverage. In particular, Sb-doped Si detectors (Si:Sb) can cover the spectral band from 15 to 31 μm with a peak response at 27 μm. When mated to a suitable readout circuit, a responsivity >3 A/W and a total read noise of less than 130 rms electrons has been demonstrated at an operating temperature of 8 K[1]. These detectors require large thicknesses to achieve adequate quantum efficiency. This makes them particularly sensitive to radiation effects such as proton radiation. Protons passing through the devices create electron-hole pairs as they interact with the constituent atoms in the lattice, producing

unwanted noise and false signals in the devices. Also, proton interactions within the readout circuitry can cause fluctuations in the detector bias, which affects the responsivity of the detectors. These effects are clearly undesirable for IR astronomy applications.

Currently under development are IBC extrinsic Si IR detectors that have several potential advantages over standard photoconductive (PC) devices. The impurity band devices are much thinner than the corresponding PC devices and thus are less sensitive to radiation effects. Also, the IBC devices do not display some of the other negative effects observed in standard PC devices such as the hook effect and long-time constants. The most promising devices tested to date are Si:As IBC devices that can effectively cover the 12- to 24-μm spectral band.

The Si:Sb detectors and the Si:As IBC devices fabricated in a 58 × 62 staring array format have been chosen for the flight experiment. The Si:Sb devices reach the longest cutoff wavelength of all the Si detectors. To date, no Si:Sb IBC devices have been demonstrated. The Si As detectors provide a look at the devices that will eventually replace the PC devices.

4.3.2.1 Description of Detectors.

Si:Sb. Si:Sb detectors are fabricated from Czochralski-grown Si doped to approximately 4×10^{15} cm^{-3} with Sb. The usual concerns regarding residual shallow impurities in extrinsic Si detectors are not important in this case, since the Sb level is shallower than the residual impurities B and P. The only concern here is that the residual B concentration be as low as possible so that it does not compensate the Sb. Double-sided polished wafers with thicknesses of 300 μm are used to fabricate the detector arrays. Both surfaces are ion-implanted with P, followed by an Al deposition to provide ohmic contacts. The Al layers are delineated such that the illuminated side has windows to allow the IR radiation to pass into the material, while individual detector contacts are delineated on the opposite side.

Si:As. Si:As IBC detectors are fabricated from epitaxially grown material on undoped Si substrates. A heavily doped layer is grown on an undoped Si substrate followed by an undoped epitaxial blocking layer. Detectors are fabricated in a manner similar to that used for the bulk PC Si:Sb devices.

One of the main advantages of the IBC device is that the absorbing layer is only 15 to 20 μm thick. Normally the heavy doping would cause impurity band current to flow in the device,

thus creating a shunt current that prevents this impurity band current from flowing. The result is a device that is less sensitive to radiation effects, has a fundamental $\sqrt{2}$ improvement in signal-to-noise ratio, has an extended wavelength response, and does not display the detrimental time constant effects of an equivalent bulk PC extrinsic Si detector.

4.3.2.2 Description of Readout Circuit. The Si:Sb and Si:As IBC devices can be In bump bonded to a switched-FET readout/multiplexer that has been used by several groups in the IR astronomical community.[1-3] A detailed description of the operation of the Si:Sb with this readout circuit and a characterization of its performance for space-based astronomy are described elsewhere.[1,4] This direct readout (DRO) is an n-channel Si MOSFET switching device with two parallel outputs. Unit cell pairs, which can be accessed in any order, are selected by means of an X,Y addressing scheme using row and column address clocks. Each unit cell of the DRO has a reset switch and source follower for each detector. In addition, there is an output source follower for each of the two outputs to drive the output lines.

4.3.2.3 Focal Plane Requirements. The FPA requirements for the flight experiment are displayed in Table 4-1. We have chosen an existing design for the array format and readout/multiplexer to minimize cost and schedule impacts on the flight experiment. As pointed out in the above discussion, a Si:Sb starring array of this format has been characterized for space-based IR astronomy applications. The operating temperature and FPA noise requirements listed in Table 4-1 are derived from these characterization data. These are reasonable requirements for the Si:As IBC devices as well. The integration time and uniformity requirements reflect the real needs of a space-based IR astronomy application. Operability is specified at a much lower level than would be required for real applications, but for the flight experiment we do not require 100% pixel operability. Lowering the operability requirements will help minimize costs of procuring the FPAs. The responsivity is chosen so that we get reasonable signal-to-noise for this experiment, but not so high as to drive the cost of procuring the arrays. Temperature stability and uniformity requirements are derived from measured temperature dependence of noise and responsivity of these types of devices. For an astronomy application in which one is trying to image a faint and distant object, the requirements would be more stringent, probably ± 0.1 K. In our experiment, we need only enough stability to observe proton events that create large signals.

Table 4-1 FPA REQUIREMENTS FOR PROTON RADIATION FLIGHT EXPERIMENT

DETECTOR TYPES	Si:Sb bulk, Si:As IBC
DETECTOR FORMAT	58 × 62
PIXEL SPACING	75 mm (center to center)
OPERATING TEMPERATURE	8 K
RESPONSIVITY AT 2 V APPLIED BIAS	
Si:Sb	>1 A/W
Si:As IBC	>1 A/W
INTEGRATION TIME	0.2-500 s
FPA NOISE/INTEGRATION TIME	100 e^- rms
OPERABILITY	>60%
UNIFORMITY OF OPERATING PIXELS	
Responsivity	±10%
Noise	±10%
TEMPERATURE STABILITY	±0.5%
TEMPERATURE UNIFORMITY OVER FPA	±0.5 K
NOISE LEVEL AT RECORDING INSTRUMENT	200 e^- rms
POWER DISSIPATION PER PIXEL	<5 μW
CABLE BETWEEN FPA AND DRIVE ELECTRONICS	
Noise Issues	
For lengths greater than 0.6 m, line drivers will be required	
Type of cable	35-wire ribbon cable/array
Low Impedance Ground	1/Array
COLD FINGER AREA REQUIRED TO MOUNT 2 FPAs	5 × 10 cm

We propose using two of each type of FPA on this experiment. This plan will increase both reliability and the volume of data collected. With a slight loss in reliability, two other detector technologies could easily be accommodated in the HELD experiment tunnel. Candidate detector technologies are: InSb at 4 K and Ge:Ga operated at 2 K.

The clocks and biases required to run the FPA will be mounted on the exterior of the cryostat. FPA-to-electronics cabling will be heat sunk at an intermediate temperature of 50 K to reduce heat losses. In addition to the operating electronics, an infrared radiation source will be included in the cryostat for responsivity measurements. A joule heated thin-film Si resistor will be used for the IR signal source.

4.3.2.4 References.

1. McKelvey, M. E., et al., "Characterization of Direct Readout Silicon:Sb and Silicon:Ga Infrared Detector Arrays for Space-Based Astronomy," *Proc. Soc. Photo-Opt. Instrum. Eng.*, Vol. 868, 1987, p. 73
2. McLean, I. C., *Proc. Workshop on Ground-Based Observations With Infrared Array Detectors*, Hilo, Hawaii, Wynn-Williams, C. G., and Becklin, E. E., eds., p. 180, 1987
3. Fowler, A. M., et al., *Proc. Workshop on Ground-Based Observations With Infrared Array Detectors*, Hilo, Hawaii, Wynn-Williams, C. G., and Becklin, E. E., eds., p. 197, 1987
4. Orias, G., and Campbell, D., "Development of 30-μm Extrinsic Silicon Multiplexed Infrared Detector Array," NASA Contractor Report 177, 446, 1986

4.4 EXPERIMENT IMPLEMENTATION

4.4.1 Mechanical/Cryogenic System

In order to provide the required thermal environment for the FPAs, the experiment will be integrated into the instrument tunnel of the LMSC project HELD. HELD is an independent development project that has demonstrated LMSC's superfluid helium capabilities. Some details of HELD are shown in Fig. 4-1.

HELD provides a convenient design that allows easy access to experiments installed in its instrument well and would allow experiments that require SFHe cooling to be integrated into a larger experiment package that would require only one flight. The purpose of this dewar is to demonstrate long-term storage of SFHe in orbit for a variety of purposes. By using technological advances such as improved multilayer insulation and a new support strut system called the Passive Orbital Disconnect System (PODS), a multiyear SFHe storage system has been developed.

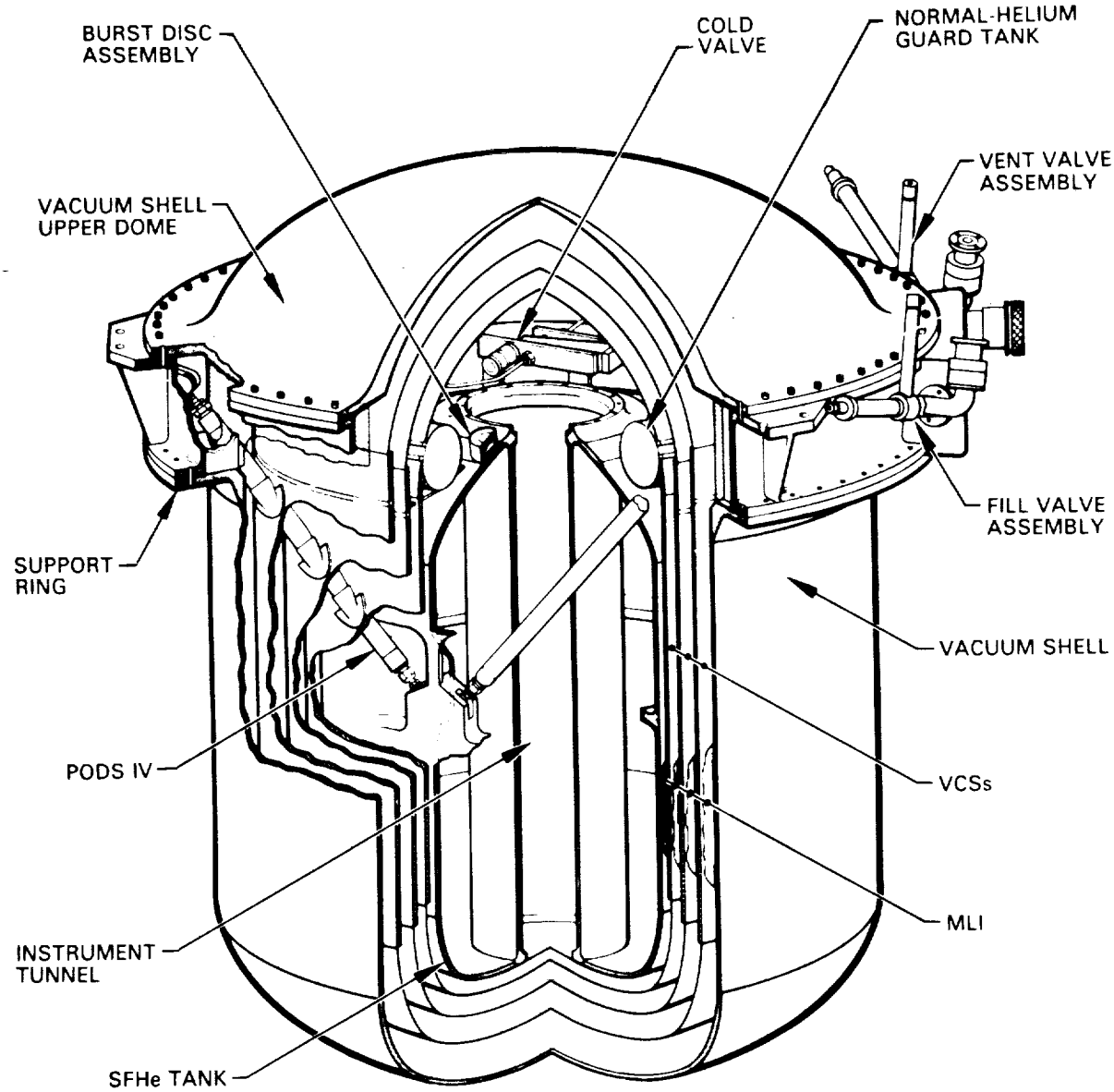

Fig. 4-1 HELD

The support system for HELD is PODS, an advanced, low-conductance support system that has been extensively tested on the ground but not yet tested in space. Concern about PODS and the possible dynamic coupling between sloshing liquid helium (LHe) has led to the suggestion that a flight demonstration/investigation be conducted since this coupling cannot be measured or fully investigated on the ground. Therefore, in addition to serving as a testbed for the FPAs, using HELD will allow characterization of the dynamic properties of

PODS in a low-gravity environment. Results of the characterization of the PODS in-orbit dynamic response can be applied to other liquid-cryogen cooling/storage systems. HELD and PODS have been designed and built and are currently undergoing extensive thermal and structural testing. (In-space testing of HELD is described in "Integrated Cryogenic Experiment (ICE) Microsphere Investigation," NASA Contractor Report 177538.)

Many specific technologies will be demonstrated by using HELD in support of experiments such as

(1) PODS

(2) Improved multilayer insulation (MLI)

(3) Low-conductance fill line

(4) Porous-plug vent

(5) PODS-supported vapor-cooled shields

(6) Simplified prelaunch servicing

The experiment package is designed to be mounted inside the superfluid cooled tank of HELD. The design of HELD permits the package to be mounted and demounted by removing the vapor-cooled shields and folding back some insulation. The experiment chamber will share a common vacuum with HELD. Instrumentation wires can be routed down PODS to minimize heat loads. Hermetically sealed connectors in the vacuum shell mounting ring of HELD provide the interfacing with flight electronics. The FPA drive electronics and signal A/D converters will be attached to the vacuum shell mounting ring. The remaining electronics will be housed in an HH-G canister.

The HELD instrument tunnel provides a 2 K environment. The focal planes will be operated at 8 K. In order to reduce heater power to achieve this temperature, the FPAs will be mounted on an Al platform thermally isolated from the 2 K sink with fiberglass/epoxy stand-offs. The FPA intermediate temperature stage is shown in Fig. 4-2.

Another experiment chosen for the outreach program will share the instrument tunnel with the FPA experiment. This experiment will characterize the thermal properties of glass microspheres. The FPA intermediate temperature stage will be mounted on the microsphere experiment canister. The integration of the two experiments is shown in Fig. 4-3.

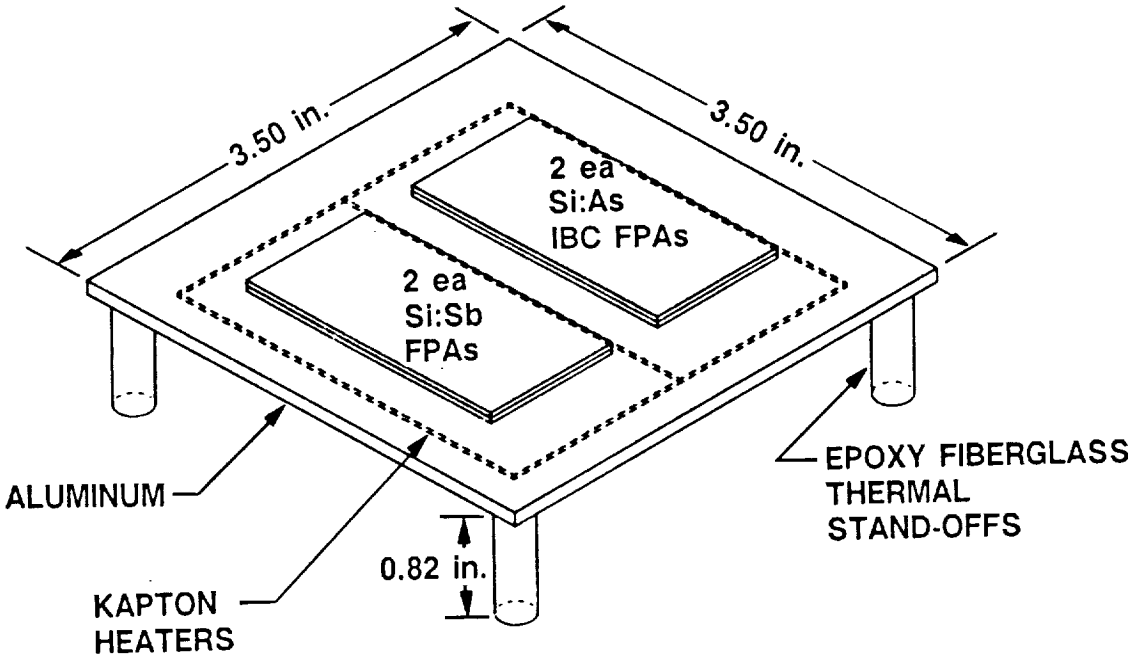

Fig. 4-2 FPA Intermediate Temperature Stage

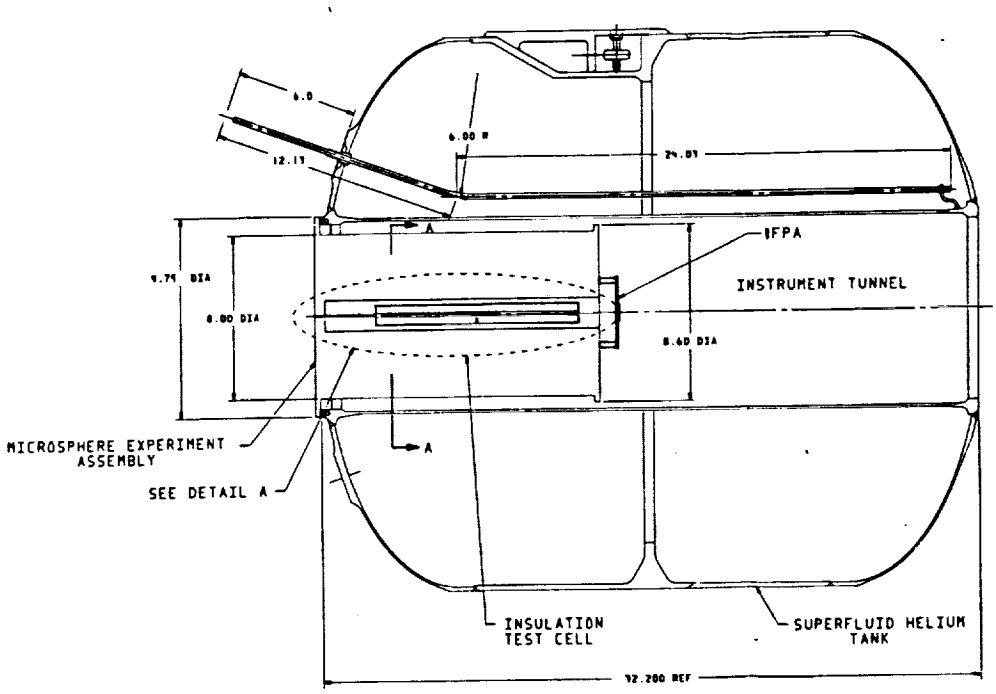

Fig. 4-3 IFPA/Microsphere Assembly

The four FPAs require 140 electrical leads (which may have resistances as high as 200 Ω), and four leads (which must have resistances less than 20 Ω). Using 44-gage Ni wire for the high-resistance leads and 44 gage Au wire for the low-resistance leads, we compute a heat load of about 22 mW. The 1500 Ω resistance heaters will add another 8-mW heat load. The largest heat load will be due to focal planes themselves. The four focal planes will consume about 72 mW. The total thermal load of the experiment will then be less than 110 mW. The heat load of both experiments may be as high as 350 mW. According to Fig. 4-4, this heat load can be tolerated for a 5-day mission.

One advantage of HELD is that it offers simplified prelaunch servicing by having a normal boiling point (NBP) helium guard tank on the first vapor-cooled shield. The purpose of this guard tank is to allow the SFHe tank to be filled and valved off prior to launch. The NBP tank is then filled and provides a 4.2 K guard shield around the SFHe tank, resulting in extremely low heat rates to the SFHe. The NBP tank is allowed to vent during ground hold and can repeatedly be refilled as needed prior to launch.

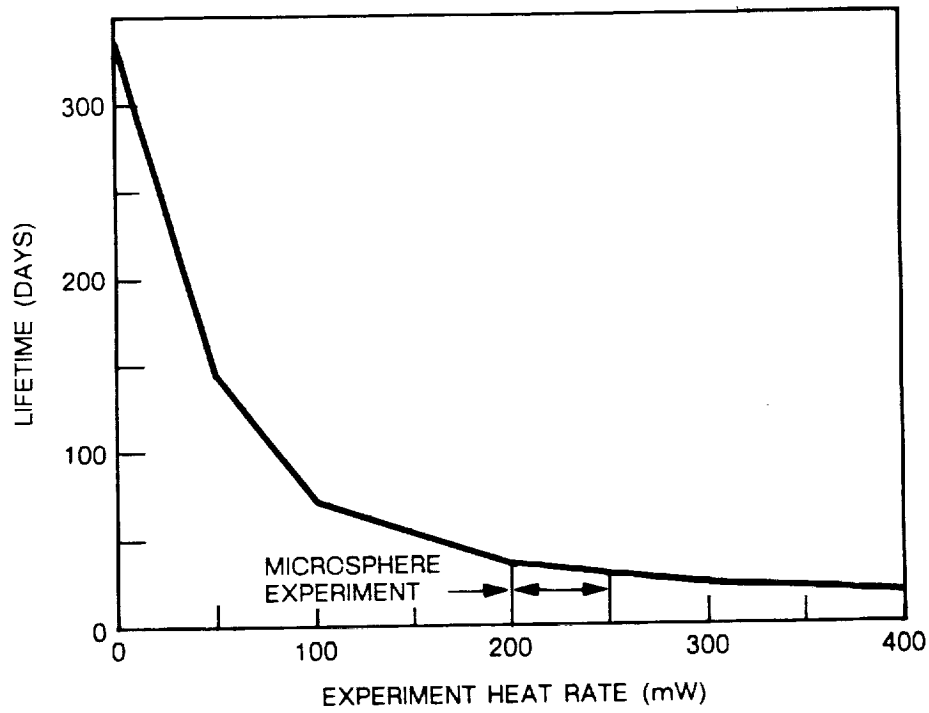

Fig. 4-4 Effect of Experiment Heat Rate on HELD Lifetime

4.4.2 Experiment Electronics

4.4.2.1 Description. The experiment electronics consists of flight- and ground-support hardware elements. The flight electronics provides control signals for the focal plane arrays, stores and encodes the experimental data, and interfaces with the orbiter's avionics package to receive uplink commands and transmit downlink data. The ground support electronics (CGSE) provides the necessary interfaces to the customer/carrier ground support equipment (CCGSE), including those to support the low- and medium-rate ground support equipment (LRGSE and MRGSE) data links. The CGSE is a workstation that enables the experimenter to monitor the health of the experiment's hardware as well as sample and control the acquisition and telemetering of data.

4.4.2.2 Installation. The flight electronics consists of two assemblies, the focal plane drive electronics (FPDE) and the data interface unit (DIU). The FPDE provides timing and control functions for the focal plane arrays located in the SFHe dewar. It consists of approximately six circuit boards and some associated power-regulation electronics. This unit will be packaged in an enclosure about 8 × 6 × 12 in. and physically located as near the arrays as possible.

The DIU provides signal conditioning, control, and telemetering functions and will be installed in a chassis mounted within one of the sealed HH-G canisters. Enclosing the DIU in one of these canisters will simplify the packaging and thermal environment management tasks and allow use of the optical disk drive, which is only rated to 50,000-ft operating altitude. Using the canister will require the design and approval of a modified canister baseplate. The modification is necessary to add at least one additional connector to interface the DIU to the FPDE. Both units will be mounted with the SFHe dewar as part of a single assembly located on the Hitchhiker-M structure. Approximate weights of the two units are: FPDE, 40 lb; DIU, 210 lb including the insulated HH-G canister.

The DIU hardware will consist of three subassemblies: an erasable/rewritable optical disk drive, an electronics subchassis, and a power supply/filter assembly, plus some interconnect cable. The disk drive is a severe environment unit and will require no additional vibration or shock isolation in its mounting. The electronics circuitry will be arranged on seven circuit boards (five different types) installed in the electronics subchassis as plug-in modules. Circuit-board functions will be as follows:

(1) Central timing and sequencing controller

(2) Disk controller and program memory

(3) Analog-to-digital converters (three identical circuit boards)

(4) Telemetry data encoder

(5) Focal plane array and environmental heater control

The DIU chassis will also contain a power supply/filter assembly, converting 28 V dc orbiter power to the dc voltage levels required for the disk drive and the electronics and providing power to the FPDE. This assembly will also contain any power devices required for driving environmental heaters.

Power consumption for the total flight system will not exceed 175 W: 50 W for the FPDE and 125 W for the DIU. There may be additional power requirements for heaters within the two electronics assemblies.

The CGSE will consist of a PC AT equivalent, with keyboard, floppy and hard disk drives, monitor, and printer. The equipment will also include a serial data decommutator compatible with the medium rate downlink output from the MRGSE. The hard disk drive will be a SCSI-compatible high-speed device which will be capable of storing at least 300 Mbyte of downlink data. The CGSE will be packaged either as a portable unit or in a small, rack-mountable assembly.

4.4.2.3 Operation. A block diagram of the system electronics appears as Fig. 4-5. There are four focal plane arrays. Each array consists of 58 × 62 elements; each array is completely read five times per second. Two elements in each array are sampled simultaneously, producing a total of eight analog outputs at each sample time. This results in eight serial analog data streams clocked at an 8.99 K word/second rate. Each analog signal is converted to a 12-bit digital data word and written to a digital storage medium.

The time for one complete experiment sample, or pass, totals 15 min, with three passes occurring per day. The data collected form the four arrays during one pass total 64.8 M 12-bit words, the equivalent of 97.1 Mbyte.

The data-storage medium will be an erasable/rewritable optical storage disk. Its capacity is 300 Mbyte, enough to store one day's data. Since the mission time will exceed one day,

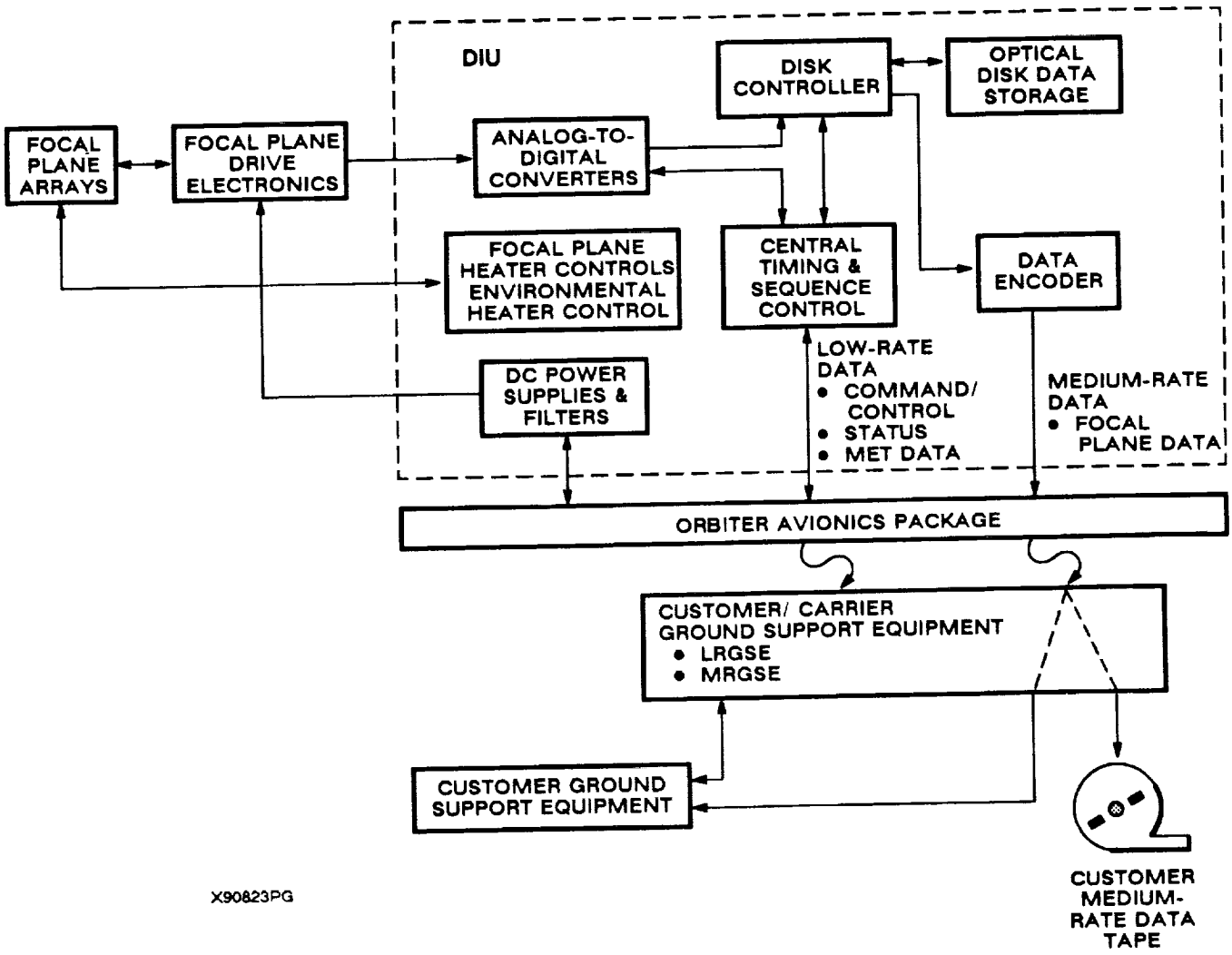

Fig. 4-5 Block Diagram of System Electronics

some means must be provided to downlink data in order to clear space on the disk. To perform this function, data bytes are read from the disk to the data encoder, which assembles them into a telemetry format compatible with the medium rate KU-band downlink; it also merges selected housekeeping status data and mission elapsed time (MET) with the array data to form the telemetry data frame shown in Fig. 4-6.

Each telemetry frame contains 462 12-bit words (5544 bits); it takes eight telemetry frames to downlink the data from one focal plane array. To downlink the full amount of array data (four arrays) from one experiment pass will require transmitting 799.2 M bits. That is, for example, 20 min of downlink time at 666 K bit/s, which will be required every 8 h.

Although the medium rate data will be collected on tape by the MRGSE, the CGSE will be capable of decommutating the MRGSE serial data and clock outputs in order to monitor the condition of the focal plane, dewar, and flight electronics systems. The CGSE will be capable of storing a limited amount of downlink data on disk to allow near realtime analysis of the focal plane data. The CGSE will also support the RS-232 synchronous up- and down-links in order to pass command data to the flight electronics.

4.4.3 Preflight Tests

The Sensor Electronics Department at LMSC's Research & Development Division has a complete focal-plane test and analyses facility. These facilities will be available to this program. All the requisite peripheral equipment such as test dewars and pumping stations are also available. A low-background test chamber with two cryogenic blackbody sources and two cryogenic filter wheels is under construction and will be available to the program. One of three FPA test stations is shown in Fig. 4-7. In this view, the FPA is cooled with an

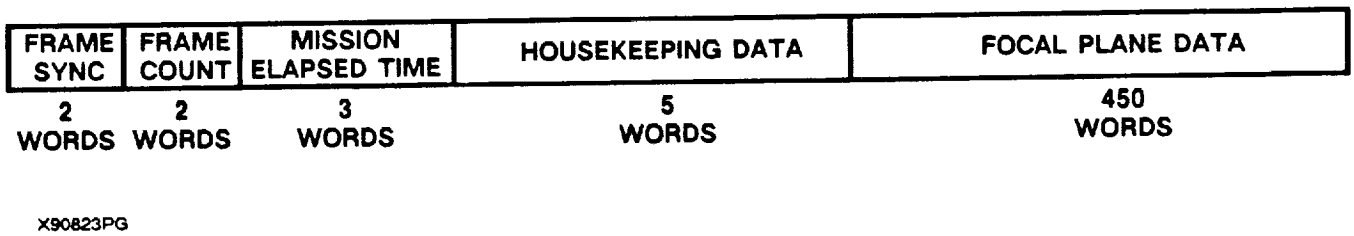

Fig. 4-6 Medium-Rate Downlink Telemetry—Frame Format

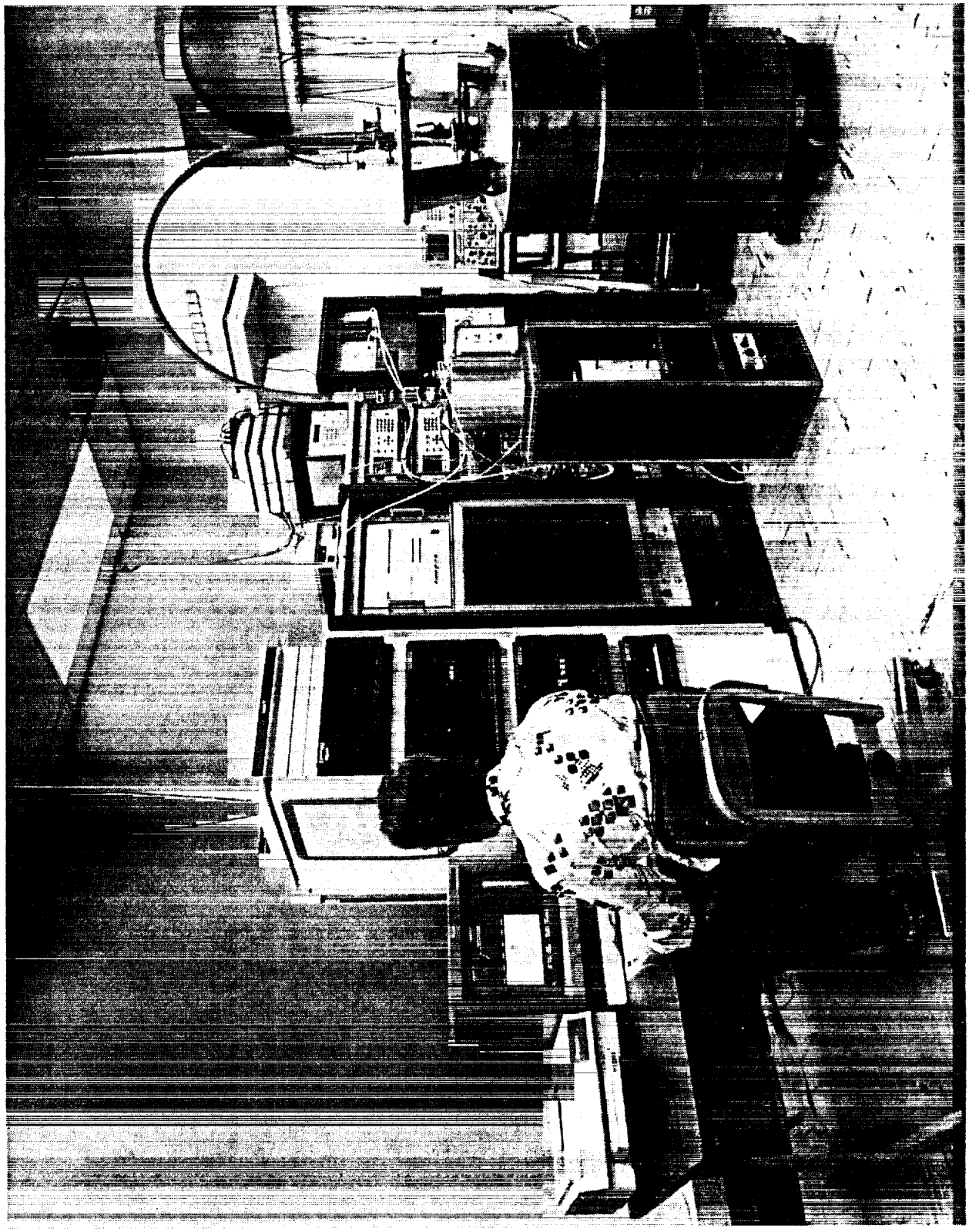

Fig. 4-7 FPA Test Station

open-cycle He refrigerator. A block diagram of the system is shown in Fig. 4-8. This general-purpose test facility has been used to characterize InSb, HgCdTe, and Si:XX FPAs.

After delivery of the FPAs, the supplier's FPA characteristics will be corroborated and the optimum operating conditions will be estimated. These tests will use the FPA test facility drive electronics. The response of the FPA to discrete ionizing events will be tested using an in-house Co^{60} gamma source. Tests will be performed at dose rates low enough not to introduce any long-term dose effects.

Initially, the focal plane drive electronics will be tested independently of the FPA. After verification of required performance levels, the electronics package will be integrated with the FPA and full-scale performance checks of the system will be conducted. These tests will include additional Co^{60} gamma tests to determine the response of the system to discrete ionizing events.

Similarly, the remainder of the flight electronics package will first be tested without the FPA and FPDE to verify performance. Finally, full system-level tests will be performed. These tests will include Co^{60} gamma-pulse testing.

The final tests at LMSC will be performed after the FPA system is integrated into HELD. These tests will include long-term thermal stability and thermal response time in addition to electrical performance tests.

4.4.4 Integration With Host Spacecraft

HELD and accompanying flight electronics will be mounted on one of the new extension capabilities of the Space Transport System (STS), the HITCHHIKER-M (HH-M). The HH-M, developed by Marshall Space Flight Center (MSFC), is a standardized mechanical platform which will carry up to 1200 lb of customer equipment mounted on a cross bay bridge type structure in the Space Shuttle. The HH-M will also be equipped with an avionics control unit that gives the customer easy access to the orbiter's resources from which a total system can be configured.

HELD is shown installed in HH-M in Figs. 4-9 and 4-10. The dewar will occupy the top of two bays of the HH-M. The two HH-M bays can accommodate 760 lb for this configuration. Table 4-2 lists the HELD component weights for the system. The flight electronics box is not shown, but it will mount on the front of the HH-M, which can support 170 lb.

X90823_FJ_4

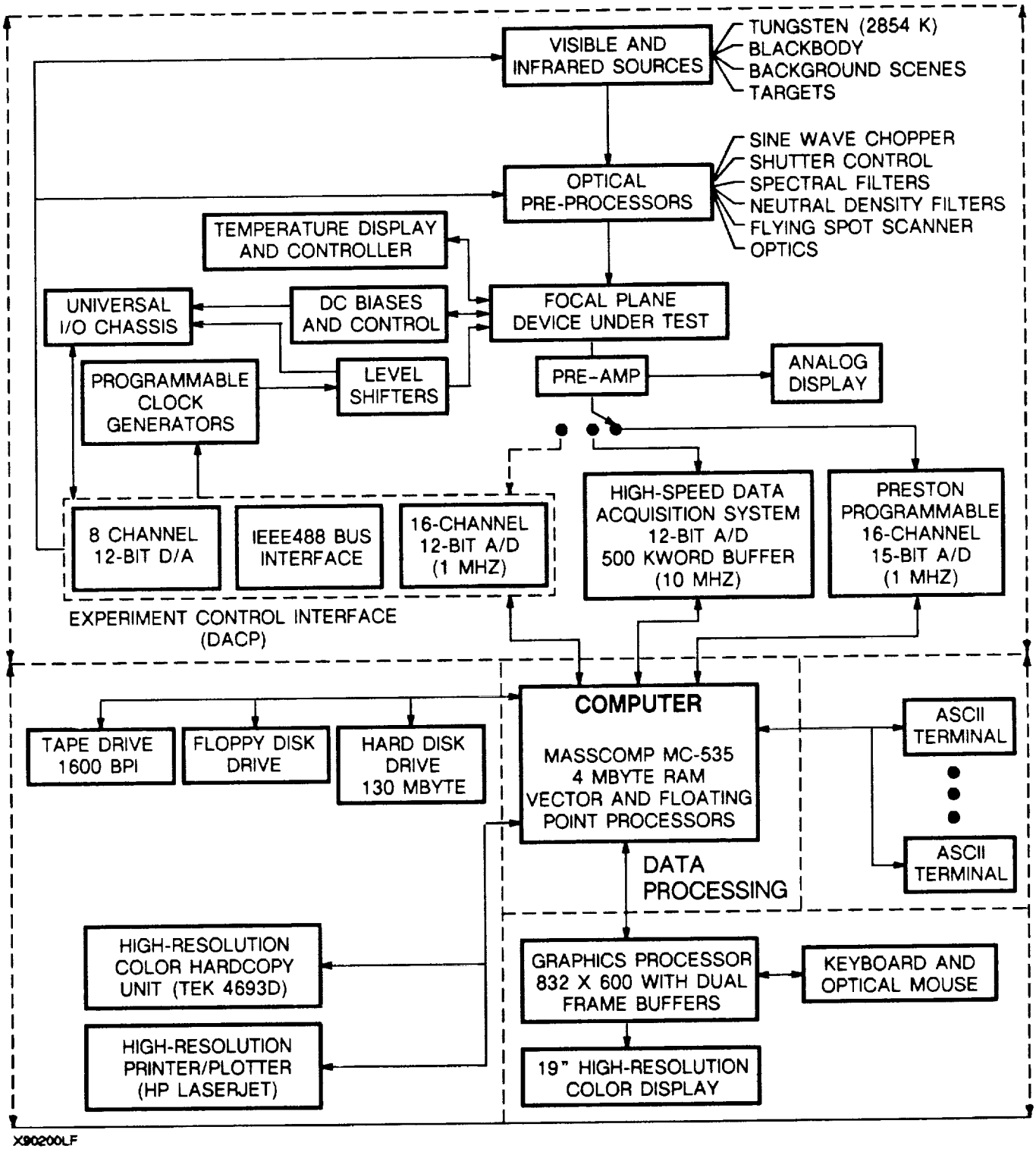

Fig. 4-8 High-Speed Focal-Plane Test Station

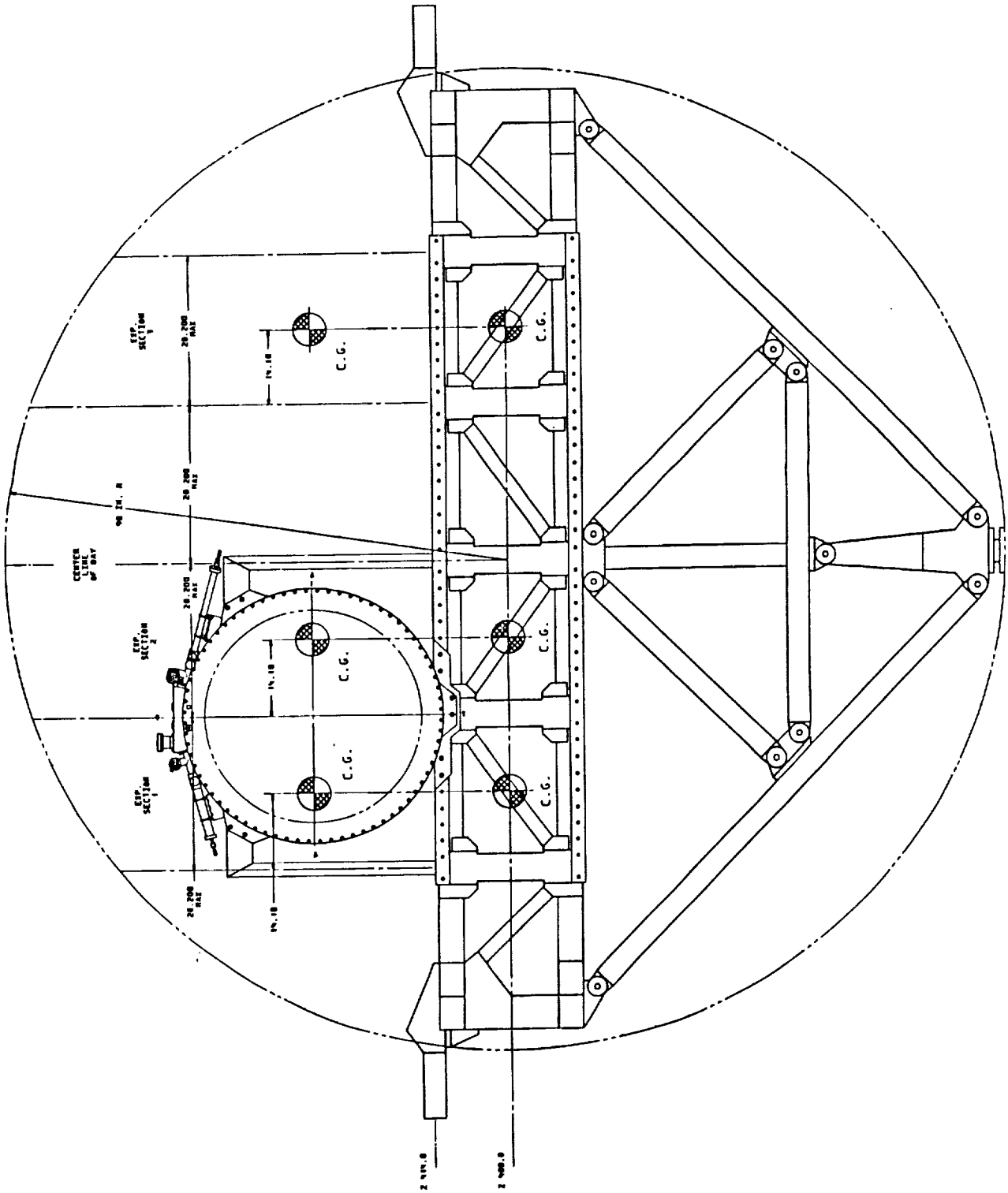

Fig. 4-9 HELD-HHM Integration (Front View)

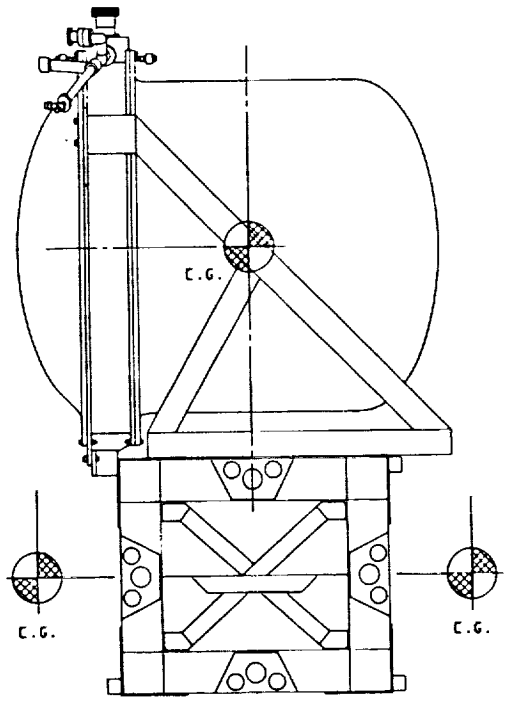

Fig. 4-10 HELD-HHM Integration (Side View)

4.4.5 HELD Testing, Fluid Management, and Safety

These subjects are described in detail in the ICE final report previously referenced.

Table 4-2 WEIGHT SUMMARY (lb)

He-II Tank and Plumbing	106
200 L He-II	55
He-1 Tank	9
15 L He-1	2
Vapor-Cooled Shields (3)	66
MLI	25
PODS (6)	8
Support Ring	52
Vacuum Ring	102
External Plumbing	5
Miscellaneous	10
Total HELD Launch Weight	440
FPA Experiment Package	1
FPA Experiment Electronics	250
Microsphere Experiment Package	25
Microsphere Flight Electronics	30
HH-M Interface Support Structure	50
Total Launch Weight (lb)	796

Section 5

PRELIMINARY COST ANALYSIS

In this section we present a preliminary cost analysis for the flight experiment Infrared Detector Performance in the South Atlantic Anomaly. The cost analysis is based on the following Work Breakdown Structure (WBS). This cost analysis addresses only those tasks directly related to this experiment. Testing HELD and its integration was presented in "Integrated Cryogenic Experiment" (NASA Contractor Report 177538).

5.1 MANAGEMENT

This includes the program controls on cost and schedule (including subcontractor cost and schedule), configuration management, administration, and technical publications.

5.2 PRODUCT ASSURANCE

This includes safety, reliability, quality assurance engineering, and inspection.

5.3 ENGINEERING AND DESIGN

This includes all the analyses necessary to complete the design of the experiment, specifications for focal plane arrays, design electronics, and experiment integration.

5.4 MANUFACTURING

This includes all the labor and materials necessary to fabricate and assemble the flight experiment.

5.5 TEST

Includes all testing, data reduction, and documentation of subsystem, system, and flight tests.

5.6 GROUND SUPPORT EQUIPMENT

This includes design, fabrication, and assembly of all fixtures, handling equipment, service equipment, and containers necessary for the experiment.

5.7 PAYLOAD INTEGRATION

This is primarily the labor necessary to support the integration of the experiment with HH-M and the shuttle.

A more detailed WBS is shown in Fig. 5-1. The schedule for the proposed 33-month program is shown in Fig. 5-2. A cost breakdown by WBS task is shown in Table 5-1. The estimated cost of the program is $3,037,149.

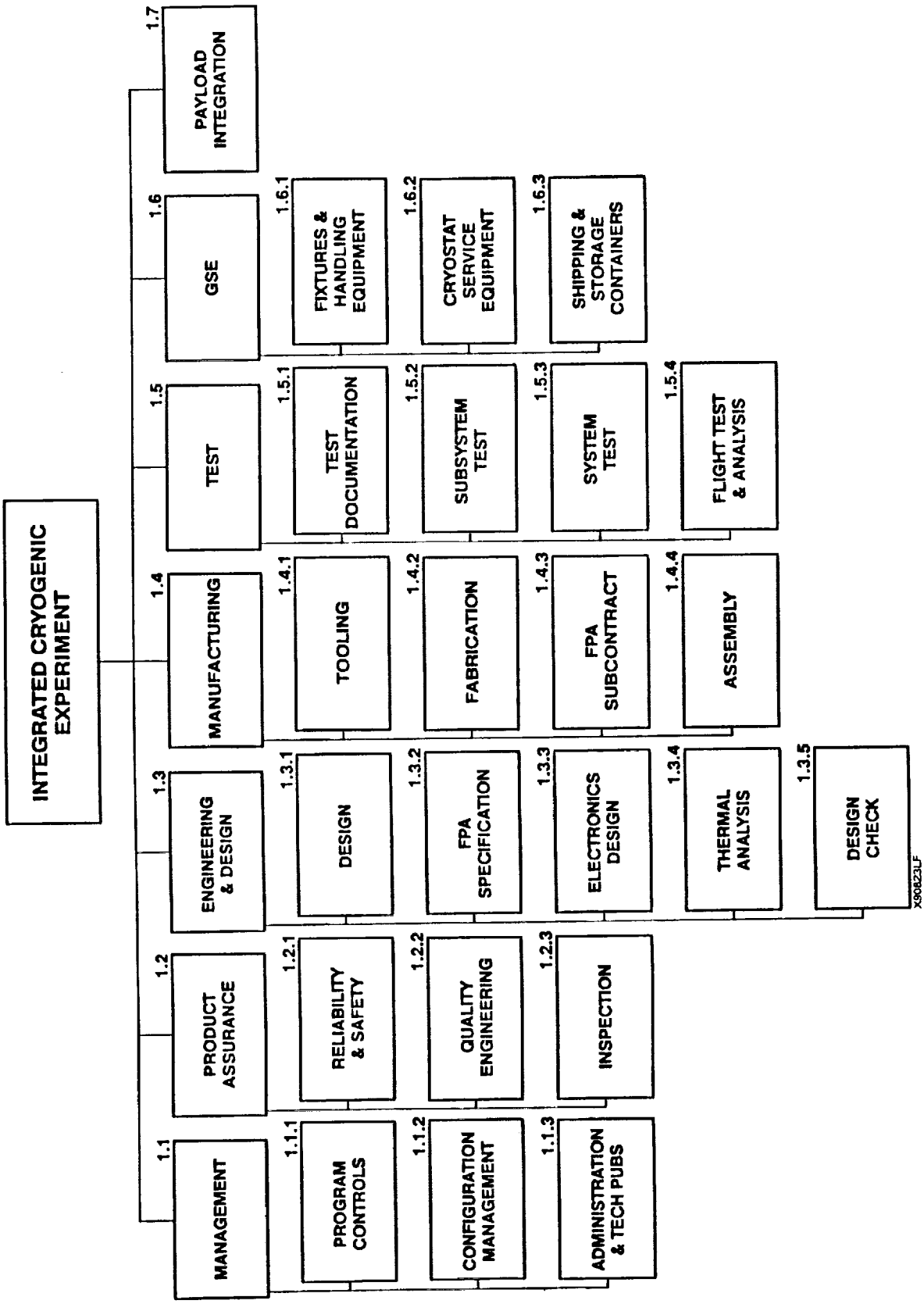

Fig. 5-1 Work Breakdown Structure

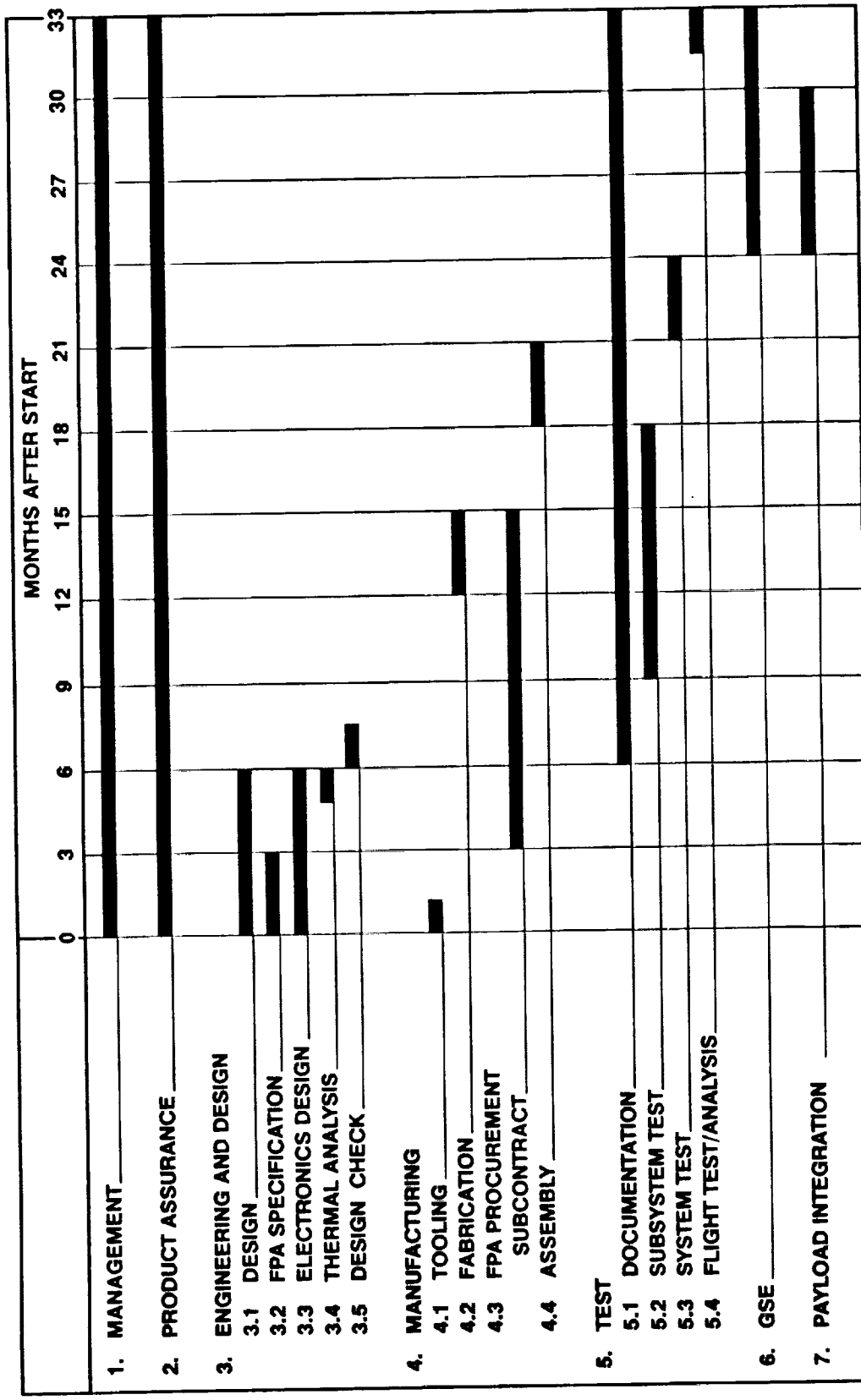

Fig. 5-2 FPA Experiment Schedule

Table 5-1 ESTIMATED MANPOWER AND COST BREAKDOWN

1.1	Management	5280 hours	
1.2	Product Assurance	2640	
1.3	Design	2400	
1.4	Manufacturing	1440	
	1.4.3 Subcontract*		$1M
1.5	Test	4640	
1.6	GSE	1040	
1.7	Payload Integration	1920	
	TOTAL	19,360	

Total Cost Excluding Fees: $3,037,149

*For four focal plane arrays
Significant savings accrue if detector arrays being developed for NASA programs are Government-furnished equipment (GFE).

Appendix A

CHORD LENGTH AND PULSE HEIGHT CALCULATION SUMMARY

The paper by Bradford[3] gives a general expression for the sum distribution of chord lengths, $C(\ell)$, in an arbitrary rectangular parallelepiped of dimensions $h \times a \times b$, where $h \leq a \leq b$. The sum distribution is the probability that a chord will be of length greater than ℓ. The chord length density, $c(\ell)$, the probability that a chord will have length between ℓ and $\ell + d\ell$, is the negative of the sum distribution with respect to the chord length, ℓ

$$c(\ell) = -\frac{d}{d\ell} C(\ell)$$

Bradford gives only expressions for the sum distribution, and plots the sum distribution as a function of chord length for various objects.

Kellerer[2] gives general expressions for calculating both the sum distribution , $C(\ell)$, and the probability density, $c(\ell)$. These expressions are

$$C(\ell) = 2k \int_d^1 \left[\frac{hx^2}{\sqrt{(1-x^2)}} F(\ell x) + xF^*(\ell x) \right] dx \qquad (1)$$

$$c(\ell) = 2k \int_d^1 \left[\left[\frac{hx^3}{\sqrt{(1-x^2)}} - x^3\ell \right] f(\ell x) + 2x^2 F(\ell x) \right] dx$$

$$+ \frac{2kh^2}{\ell^3} \int_{\sqrt{(\ell^2-h^2)}}^{\infty} F(x)dx \qquad (2)$$

The second integral in $c(\ell)$, expression (2), applies only when $\ell \geq h$, and is zero otherwise.

Here

$$d = 0 \text{ for } \ell \leq h$$

$$= \sqrt{(1 - h^2/\ell^2)} \quad \text{for } \ell > h$$

$$F(t) = \int_t^\infty f(x)\, dx$$

$$F^*(t) = \int_t^\infty F(x)\, dx - tF(t)$$

f(t) is the two-dimensional probability density for a chord of length t in a rectangle of dimensions a × b. This is calculated for the specific geometry, as in Coleman,[1] and, in our case of a rectangular cross section, a × b, to our parallelepiped is given by[3]

$$f(t) = \frac{1}{a+b} \qquad \text{for } 0 < t \leq a$$

$$= \frac{a^2 b}{t^2(a+b)(t^2-a^2)^{1/2}} \qquad \text{for } a < t \leq b$$

$$= \frac{ab}{t^2(a+b)} \left(\frac{a}{(t^2-a^2)^{1/2}} + \frac{b}{(t^2-b^2)^{1/2}} - \frac{t^2}{ab} \right)$$

$$\text{for } b < t \leq \sqrt{(a^2+b^2)}$$

$$= 0 \qquad \text{for } \sqrt{(a^2+b^2)} < t$$

It is from expression (1) that Bradford derives his analytical expressions for the sum distribution.

Bradford gives individual solutions for the sum distribution for four regions of the chord length, ℓ, related to the dimensions, h, a, and b, of the region in which the chord length distribution is to be found. These regions are

(1) $0 < \ell \leq h$

(2) $h < \ell \leq a$

(3) $a < \ell \leq b$

(4) $b < \ell \leq \ell max$

where $lmax = (a^2 + b^2 + c^2)^{1/2}$

There is an error in the expression for the sum distribution in region 3 in Bradford's paper.

Bradford's expressions for the sum distribution may then be differentiated with respect to the chord length to obtain analytical expressions for the probability density, $c(\ell)$. This was attempted, but the results were disappointing due to the excessive time required to correct Bradford's sum distribution expressions and to derive the probability density from them.

Rather, we used the alternative method of calculating sum distribution and probability density values directly from expressions (1) and (2) by numerical integration. In this case, it is seen that since

$$f(t) = 0 \text{ for } t > \sqrt{(a^2 + b^2)}$$

the upper limit of the integration in the expressions for $F(t)$, $F^*(t)$, and $c(\ell)$ becomes

$$\sqrt{(a^2 + b^2)}$$

The numerical integration was performed by the quartic analog to the Simpson's Rule method.

The numerical integration program gave sum distribution results which matched those of Bradford for the case of a cube of side 10 μ and a volume of 10 $\times$ 40 $\times$ 60 μ. The program was then employed to calculate the sum distribution and probability density for chord lengths in the 75- $\times$ 75- $\times$ 300-μ volume of interest.

At this point, we acquired the NOVICE code, which computes pulse height distributions via a Monte Carlo simulation. We stopped development of the in-house chord length calculation model when the already maturely developed NOVICE code became available.

References

1. R. Coleman, "Random Paths Through Convex Bodies," J. Appl. Prob., Vol. 6, 1969, p. 430.

2. A. Kellerer, "Considerations on the Random Traversal of Convex Bodies and Solutions for General Cylinders," Radiation Research, Vol. 47, 1971, p. 359.

3. J. Bradford, "A Distribution Function for Ion Track Lengths in Rectangular Volumes," J. Appl. Phys., Vol. 50(6), Jun 1979, p. 3799.

NASA

Report Documentation Page

1. Report No.	2. Government Accession No.	3. Recipient's Catalog No

4. Title and Subtitle
INFRARED FOCAL PLANE PERFORMANCE IN THE SOUTH ATLANTIC ANOMALY

5. Report Date
NOV. 1989

6. Performing Organization Code

7. Author(s)
Frank A. Junga

8. Performing Organization Report No
LMSC - F279280

10. Work Unit No.

9. Performing Organization Name and Address
Lockheed Research Labs
0/97-40, B202
3251 Hanover St.
Palo Alto, CA 94304

11. Contract or Grant No.
NAS2-12898

13. Type of Report and Period Covered
FINAL REPORT
23 Sept. 88 - 30 Sept. 89

12. Sponsoring Agency Name and Address
National Aeronautics and Space Administration
Washington, D.C. 20546-0001

Ames Research Center, Moffet Field, CA 94305

14. Sponsoring Agency Code

15. Supplementary Notes

16. Abstract - The objectives of this program were: (1) characterize trapped proton-induced pulse height distributions in bulk Si: XX infrared detectors, (2) measure pulse height distributions produced by cyclotron beam protons, (3) analyze experimental distributions and (4) develop a flight experiment to test pulse height distribution modeling and enlarge pulse height distribuiton data base. Pulse height distributions appropriate to Shuttle altitudes were computed using the NOVICE code. Maximum pulse heights in a 75-X75-300-μ detector were about $2X10^6$ charge pairs, independent of shielding (1gm/cm^2 to 19.3 gm/cm^2). Shielding greater than 2.7 gm/cm^2 produced negligable reductions in pulse rate. Pulse height distributions induced by a 67 MeV unidirectional proton beam had two peaks, one at $3.8X10^5$ pairs and the other at $1.2X10^5$ pairs. The larger peak is in good agreement with NOVICE calculations for a unidirectional beam. The lower peak is believed to be due to charge collection inefficiencies.

A flight experiment was developed to test pulse height distribution modeling and to compare the response of bulk SiiXX detectors with Impurity band detectors. The experiment would be performed during a 5 day Shuttle flight and would require minimal crew interatction.

17. Key Words (Suggested by Author(s))	18. Distribution Statement
Infrared Focal Planes, protons, South Atlantic Anomaloy, Pulse Height Distributions, Noise	UNCLASSIFIED - UNLIMITED

19. Security Classif. (of this report)	20. Security Classif. (of this page)	21. No. of pages	22. Price
UNCLASSIFIED	UNCLASSIFIED	64	$15.95

NASA FORM 1626 OCT 86